EVALUATION OF A DESKTOP COMPUTED RADIOGRAPHY SYSTEM FOR IMRT DOSIMETRY

A Thesis

Submitted to the Graduate Faculty of the
Louisiana State University and
Agricultural and Mechanical College
in partial fulfillment of the
requirements for the degree of
Master of Science in Medical Physics and Health Physics

in

The Department of Physics and Astronomy

by
Ines-Ana Jurkovic
B.S., University of Zagreb, 1992
M.S., University of Zagreb, 1998
December 2004

Acknowledgments

husband Miljenko Markovic, who has endured me during the research, for his constant support and encouragement.

Table of Contents

List of Tables

List of Figures

Abstract

Different techniques have been developed and used to evaluate dose distribution calculation accuracy and dose delivery reproducibility as a part of patient-specific IMRT QA – e.q. film dosimetry, ionization chambers, and diode arrays. To verify that the calculated dose distribution is delivered accurately during treatment, film dosimetry is usually used. The accuracy and reproducibility of film opti05 s7-10(andensy)29.6(5)-10(ands-10(and ind5 storf)]se di usinfluenc acb29.6(5)-selors7-variable

with approximately 7 fields per patient. Analysis of film was done with commercial IMRT analysis software. Analysis of CR plate data was done in IDL (Research Systems, Inc.), with programs written in house, and included several separate algorithms including automatic image registration. This algorithm uses the Fourier-Mellin transform for automatic image registration.

It was found that CR plates showed generally good agreement with the planned values with some significant over-response in the low dose regions, which can be reduced by filtration and improved calibration curves.

In view of the results presented, a CR system stands as a potentially fast and practical tool for IMRT patient-specific treatment QA.

Introductionoduo]TJ15.96108 745.9618 Tm13.560111 Tc[T

resulting dose distribution does not satisfy the clinical goal, the planner needs to change the way the problem is described so that the optimizer returns a better solution. The planner chooses beams (gantry positions, field size) and enters objectives; then discrete or continuously varying intensity profiles for each defined beam direction represent the calculated output.

In a multisegmented static field delivery, each field is subdivided into subfields that have uniform beam intensity levels. These subfields are created by the multileaf collimator (MLC) and delivered in a stack arrangement one at a time in sequence without operator intervention. While MLC leaves are moving to shape the next subfield, the accelerator is turned off. The final intensity profile is a composite of dose increments delivered by each subfield (Figure 1). This method of IMRT delivery is also called “step and shoot”.

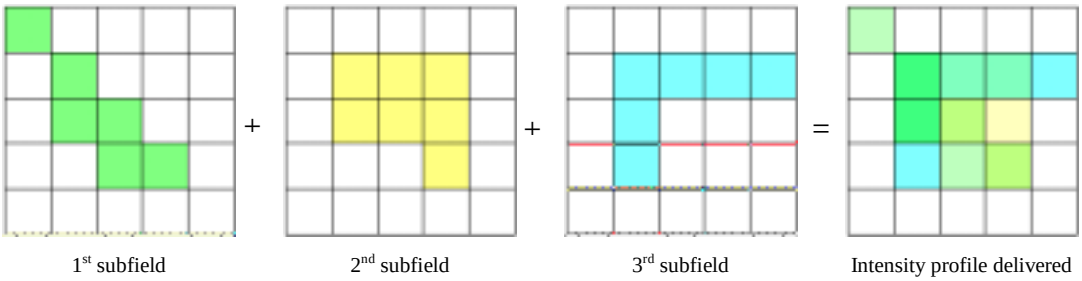

Figure 1. Intensity profile delivered from MLC sequence

For the clinical implementation of IMRT at least three systems are required:

- A treatment planning computer system;
- A system that transfers planning information to the delivery system; and

- A system for delivering the intensity profiles as planned.

Figure 2 presents a flow chart for an IMRT procedure. The process of IMRT treatment includes treatment setup (patient positioning), patient immobilization, image acquisition (CT mostly), treatment planning, treatment verification and actual treatment.

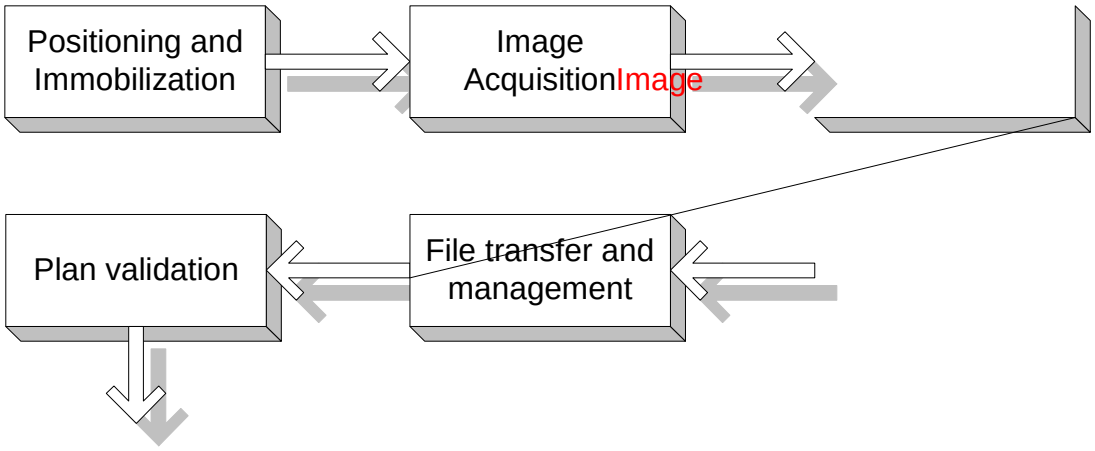

accuracy; patient-specific QA includes phantom plan measurement, fluence (intensity) map check, and absolute dose verification. In general, QA of IMRT has three aspects: commissioning and testing of the treatment planning and delivery systems, routine QA of the delivery system, and patient-specific validation of treatment plans. The first aspect is concerned mainly with the integrity of the inverse planning and IMRT delivery system. The second one is concerned with the normal operation of the MLC delivery system. The third one ensures an accurate and safe treatment of a patient.

IMRT QA requires an advanced understanding of mathematical principles of dose optimization, computer-controlled delivery systems and issues that relate to the dosimetry of small and complex-shaped radiation fields. It also requires understanding of treatment setup, planning and delivery uncertainties, and their impact on patients treated with IMRT. Treatment planning optimization for IMRT is based on dose-volume constraints and dose limits for critical structures and target tissues. Therefore, understanding these concepts is also important. Overall, QA for IMRT is much more complex than QA for conventional radiation therapy.

The goal of IMRT plan validation is to verify that the correct dose and dose distribution will be delivered to the patient as calculated by the treatment planning system. To ensure proper IMRT delivery, one needs to check that the plan has been computed properly and that the leaf sequence files and treatment parameters charted and/or stored in the Read/Verify system are correct and will be executable. Items that

verifies whether an accelerator and/or MLC controls are behaving properly, at least for the day of the study. Typical techniques used for this verification are

- film dosimetry;
- ionization chamber measurement; and
- diode array measurements.

To verify that the calculated dose distribution is delivered accurately during treatment, film dosimetry is usually used. In this case the IMRT plan verification procedure includes phantom plan calculation (extraction of planar dose distributions), phantom and film irradiation, film developing, scanning and calibration, and finally plan/film comparison.

Our question is, can a desktop computed radiography (CR) system be used for the patient-specific IMRT QA? Computed radiography is a well established process for digital radiographic imaging. In comparison to film, the main CR

Materials and Methods

A power supply provides direct current (DC) power to the modulator. High-voltage pulses from the modulator section are flat-topped DC pulses of a few microseconds in duration. These pulses are simultaneously delivered to the microwave power source (magnetron or klystron) and the electron gun. Pulsed microwaves produced in the microwave power source are injected into the accelerator tube via a waveguide system. At the proper instant electrons produced by the electron gun are also pulse injected into the accelerator structure. The accelerator tube consists of a copper tube with its interior divided by copper diaphragms of varying aperture and spacing. This whole section is evacuated to a high vacuum. As the electrons are injected into the accelerator tube with an initial energy of about 50 keV, the electrons interact with the electromagnetic field of the microwaves. The electrons are bunched together and accelerated along the accelerator tube.

As the high energy electrons emerge from the exit window of the accelerator structure, they form a pencil beam of about 3 mm in diameter. The electrons are then bent under the action of a transverse magnetic field through the angle between the accelerator tube and the target – this bend is simply a way of reducing the overall length of the machine.[1]

In electron mode the electron beam is allowed to pass through a vacuum window at the end of the accelerator and thence on towards the patient. When operating in photon mode, the electrons impinge upon a high atomic number target where bremsstrahlung photons are produced. Finally the electron or photon beam

passes through a segmented radiation detector and a variety of beam modifiers in the accelerator head before reaching the patient. Figure 4 illustrates medical LINACs operating in photon mode and electron mode.[1]

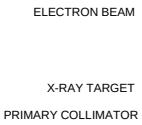

produces 6 MV and 18 MV photons; both produce five energies (6 MeV, 9 MeV, 12 MeV, 16 MeV, and 20 MeV) when used in electron mode. The 21EX model is equipped with MLCs and capable of delivering IMRT treatments. Photographs of the components of the treatment head and gantry of a Varian LINAC 21EX (6-18) are shown in Appendix A.

Multileaf Collimator (MLC)

An MLC for photon beams consists of a large number of collimating blocks or leaves that can be driven automatically, independent of each other to generate a field of almost any shape. A typical MLC system consists of 80 leaves or more arranged in opposed pairs. The 21EX MLCs have 120 leaves. An individual leaf has a projected width of 1 cm or less at the isocenter. The leaves are made of tungsten alloy and have thickness in the beam direction ranging from 6 cm to 7.5 cm, depending on accelerator type. The leaf thickness is sufficient to attenuate primary x-ray transmission through the leaves to less than 2% (compared with about 1% for collimator jaws and 3.5% for Cerrobend blocks). The interleaf transmission is usually less than 3%.[1]

the standard collimator with the MLC. Each approach has advantages and disadvantages.

MLCs can be used as a field shaper and blocking device (instead of custom blocks made of lead or Cerrobend). The use of MLCs in blocking and field shaping is ideally suited for treatments requiring large numbers of fields because automation of the blocking procedure results in a significant reduction of set-up time. MLCs can practically eliminate the use of Cerrobend blocking except for shaping small fields or "island" blocking in which an area within the open portion of the fields needs to be blocked.

The importance of MLCs is not just the replacement of Cerrobend blocking. MLCs are an essential part of beam intensity modulation for IMRT deliveries. In multisegmented static field delivery, each field is divided into subfields that are irradiated with uniform beam intensity. The subfields are created by the MLC and delivered in a segmented stack arrangement. The accelerator is turned off while the leaves move to create the next subfield. The sum of dose increments delivered by each subfield creates the intensity modulated beam as it was planned by the treatment planning system (see Figure 1). This method of IMRT delivery is called "step-and-shoot".[1]

Treatment Planning System (TPS)

At Mary Bird Perkins Cancer Center, patient and phantom IMRT plans are calculated using an ADAC Pinnacle[3] treatment planning system.

IMRT Planning and Planar Dose Extraction

The IMRT planning process consists of two components:

- Optimisation
    - During the optimisation process, desired fluences are calculated for each field to get an optimised dose distribution from the user-specified dose and DVH (dose-volume histogram) constraints for target and organs at risk.
- Conversion
    - In the conversion process, desired field fluence profiles (from the optimisation step) are translated to MLC motion patterns. Expected fluence profiles for every field are created, that take into account physical and mechanical aspects of the MLC and LINAC. These realistic profiles are used for the calculation of the final dose distribution.

After the IMRT treatment plan is approved by the physician, planar dose files for the IMRT QA are created. The planar dose option in the Pinnacle system allows generation of the dose distribution for any beam at a given depth in either a flat water

plate's advantages include ease of use, high spatial resolution, high detection sensitivity with high signal-to-noise ratio, large detection area, extremely wide dynamic range, and capability for reuse.[6]

The CR plate is made up of protective, phosphor, and support layers (structure is shown in more detail in Figure 7). The imaging plate is coated with a photostimulable storage phosphor ($BaFBr:Eu^{2+}$), that is sensitive to several kinds of radiation and is widely used in various fields.[6] The phosphor layer consists of very small crystals (grain size: about 5 μm) of photostimulable phosphor of barium fluorobromide containing a trace amount of bivalent europium as a luminescence centre; these centers are sensitive to photons in the x-ray energy range.

Photostimulated Luminescence (PSL)

Naturally or artificially irradiated minerals may emit light with decreasing intensity upon illumination, especially with excitation wavelengths longer than the wavelength of the emitted light. This effect is clearly different from fluorescence excited by shorter wavelengths or phosphorescence ceasing slowly after illumination.[7]

In 1921 Przibram observed that irradiation-coloured kunzite (rose fluorspar) crystals were bleached not only by heating, but also by light, and that in some cases phosphorescence was detectable. The observed effect of light emission of illuminated irradiated substances was described as radio-photoluminescence. During his first experiment, Przibram irradiated kunzite using a radium source and

photomultiplier tubes (PMTs). PMTs convert light into voltage signals, which are amplified and digitised. The sampling process produces 1024 pixels for each scan line. The 12-bit digital image is then transferred to the computer for image processing.[9]

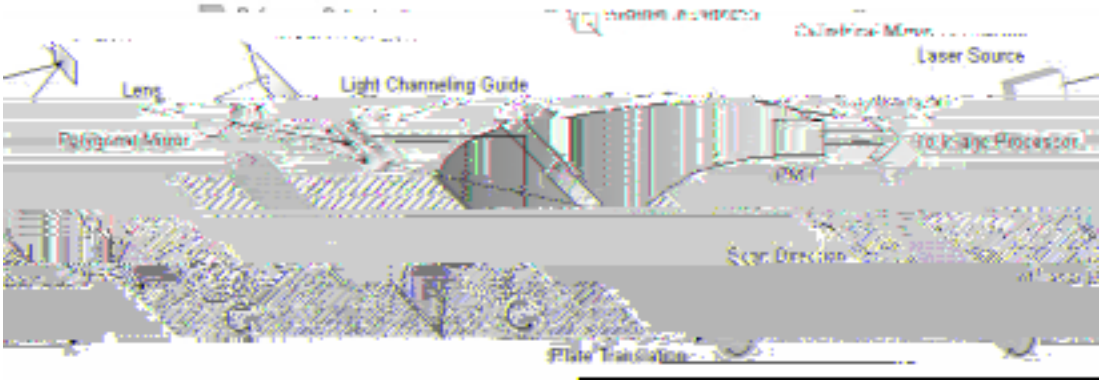

Figure 6. Latent image readout

The readout cycle of an imaging plate is illustrated in Figure 7. The imaging plate captures x-ray radiation or electrons in its phosphor crystal structure, creating a latent image. To readout an image, the imaging plate is placed in the CR scanner/reader. As the laser beam in the CR reader scans across the imaging plate, the phosphors are excited and release the energy they have stored. This energy is

processing methods. These differences were not investigated as part of this project. The CR system used in this study is a Kodak ACR-2000i system.

Kodak ACR-2000i System

The Kodak ACR-2000i system consists of a phosphor plate reader with the integrated eraser, shown in Figure 8. A darkened room is recommended for handling of CR plates. A computer workstation and Kodak General Radiography software are included as part of the system. The ACR-2000i system scans plates up to 14 x 17 in. in 50 seconds; erasure takes 30 seconds per plate. Images can be saved and exported in DICOM 3.0 format.[10]

Figure 8. Kodak ACR-2000i reader and eraser

Phantom Used in the Study

Basic dose data are usually measured in a water phantom (water tank) that closely approximates the radiation absorption and scattering properties of muscle and other soft tissues. Since it is not always possible to put radiation detectors (such as CR plate or film) in water, solid dry phantoms have been developed as water substitutes.

For a given material to be water equivalent it must have the same effective atomic number, number of electrons per gram, and mass density. Since Compton effect is the dominant mode of interaction for MV photon beams in the clinical range, the necessary condition for water equivalence is the same electron density number as that of water.

The electron density of a material, ρ_e, may be calculated from its mass density, ρ_m, and its atomic composition as

Eq. 1. $$\rho_e = \rho_m N_A \sum_i a_i \left(\frac{Z_i}{A_i} \right)$$

where N_A is Avogadro's number and a_i is the fraction by weight of the ith element of atomic weight A_i and atomic number Z_i.[1]

A common solid dry phantom is a plastic water phantom. This phantom is an epoxy resin-based mixture. It has a density of 1.02 g/cm^3 and provides dosimetry characteristics similar to natural water over the entire oncology energy range. Dose

measurements in a plastic water phantom agree with those in true water within 0.5% ± 0.04% above 7 MeV and need no correction factors.[11]

Through the course of this study, a plastic water phantom was used. Two slabs of plastic water were used, each with dimensions of 30 x 30 x 5 cm^3 (width x length x thickness).

Measurement Procedure

Setup for the Measurements

The setup used for plate exposures was the same as the setup used commonly for film dosimetry. A series of measurements with several different thicknesses of lead sheets were used (lead sheets are used as low-energy photon filters, in film dosimetry they can be used on both sides of the film to compensate for overresponse of the film to low-energy photons). Because no significant differencponb6Tm-0.00pserv0(on-0.0009 T

backing) to protect the plates from direct exposure to light and from possible damage during regular handling throughout the measurement process.

To setup a CR plate for exposure, the CR plate was first transferred from the cassette to a paper envelope. The film was placed between the two slabs of plastic water; the white surface of the CR plate faces the x-ray source. The phantom is positioned on the treatment couch. The source to plane distance (SPD) was 100 cm (location of the plate); the source to surface distance (SSD) was 95 cm. Finally, a 5 x 5 cm^2 field was used for all calibration measurements. The field sizes for the patient plan exposures varied according to the plan. All measurements were made at a depth of 5 cm. Figure 10 shows this setup.

Figure 10. CR plate exposure setup

Exposure

Exposures were made for 3 different energies: 4 MV, 6 MV and 10 MV. Calibration curve measurements were done first for each energy and then for all

three energies; IMRT fields from 10 different patients (approximately 7 fields per patient) were acquired. Some fields were repeated to check reproducibility.

Each patient plan was opened in the MultiAccess application. QA mode was chosen as the mode of delivery and the first IMRT field is selected in the resultant window. Once the chosen field was downloaded MLCs started to move to shape the appropriate area. After the exposure (delivery of the chosen field), proof of the delivery is recorded as QA performed. The next field is chosen afterwards.

After the delivery of each field, the CR plate was taken out of the treatment room, still in the envelope, and scanned in the Kodak scanner. For study purposes, some of the plates (where noted) were scanned immediately after exposure and some after various time intervals.

Scanning

After the exposure the plate is taken out from the envelope and placed in the scanner. On the Kodak computer a new study is created and with the click of a button the plate is scanned. During the scanning process, the image slowly appears on the computer screen as it is being read by the scanner system.

The scanning was done in port film mode. Port film mode uses a photomultiplier tube gain reduced by 100 in comparison to when used in diagnostic mode. Low resolution mode (1024 pixels) setting was used. With this setting, average image size was 2.5 MB. The Kodak software saves plate images in DICOM

3.0 format. After the plate is read, it falls into a drawer where it gets erased with a bright halogen light. After a few seconds the plate is ready for reuse.

DICOM

DICOM (Digital Imaging and Communications in Medicine) is a standard that is a framework for medical-imaging data transfer. Based upon the Open System Interconnect (OSI) reference model, which defines a 7-layer protocol, DICOM is an application-level standard, which means it exists inside layer 7 (the uppermost layer). The standard was developed by the American College of Radiology (ACR) and the National Electrical Manufacturers Association (NEMA) with input from various vendors, academia, and industry groups. It is referred to as "version 3.0" because it replaces versions 1.0 and 2.0 of the standard previously issued by ACR and NEMA, which was called the "ACR-NEMA" standard. DICOM provides standardized formats for images, a common information model, application service definitions, and protocols for communication.[12] Kodak uses the DICOM 3.0 standard for storage of the image data.

To use DICOM images in available programs all file name extensions had to be changed to accommodate different file name conventions. An MS Visual Basic script was developed for this purpose.

Reading in, Conversion and Calibration of Plate and Plan Image Files

Conversion of Plate Image Files

During the course of the study, the decision was made to read in and compare, in the algorithm developed for the IMRT analysis, both plan and plate images in TIFF format. For that purpose, a program for the conversion of Kodak DICOM files to TIFF files was developed in MS Visual Basic (VB). The program uses Kodak Image Controls, DICOM ocx[13,14] (DICOM ActiveX control), and Microsoft Common Dialog Control as part of the VB project components.

The program (see Appendix B) is capable of opening original Kodak DICOM 3.0 files. The program converts the image to TIFF format and can also perform several transformations. Transformations include grayscale inversion and flipping it horizontally and/or vertically. The program can also be used simply to change the extension of the original DICOM file.

Every acquired plate image had to be opened in this application and converted to TIFF format. Because such a large number of exposures was made (around 700), this process was not very efficient. Taking this into consideration, we switched to using a free DICOM reader program called IrfanView[15] for the plate DICOM image to TIFF format conversion. Because this software requires DICOM files to have .dcm extension, the Visual Basic script was used for file renaming.

This renaming script changes the KODAK DICOM file name to a user specified name with the .dcm extension, Figure 11.

Conversion and Calibration of Plan Image Files

Plan Calibration Curve

The TPS field (plan) image contains information on dose rate values; to get dose (in cGy), one multiplies those values by the number of monitor units actually delivered by the LINAC when delivering the plan to the phantom. For convenience, the commercial RIT113 software[16] was used (instead of developing an equivalent program in-house).

For every plate exposure, for each field delivered, a plan calibration curve is required by our IMRT analysis algorithm. The calibration maps dose (in cGy) to pixel values or shades of gray. To generate the calibration curve, the minimum, middle and maximum dose rates were obtained from the RIT113 software and multiplied by the number of monitor units. These dose values were linearly scaled across 255 pixel (gray) levels, with the minimum value mapped to a pixel value of 0 and the maximum mapped to 255. MS Excel was used to calculate the slope and intercept of the calibration curve from these values. Figure 12 shows a sample plan image and a color bar indicating the dose rate values. Table 1 and Figure 13 give the conversion values and linear calibration for this sample plan, which required 184 monitor units to be delivered.

The plan image calibration procedure is repeated for all the fields delivered for each patient. Approximately 300 different fields were delivered in this study.

The coefficients for the linear calibration are used subsequently in the algorithm for the conversion of the plan image to dose values.

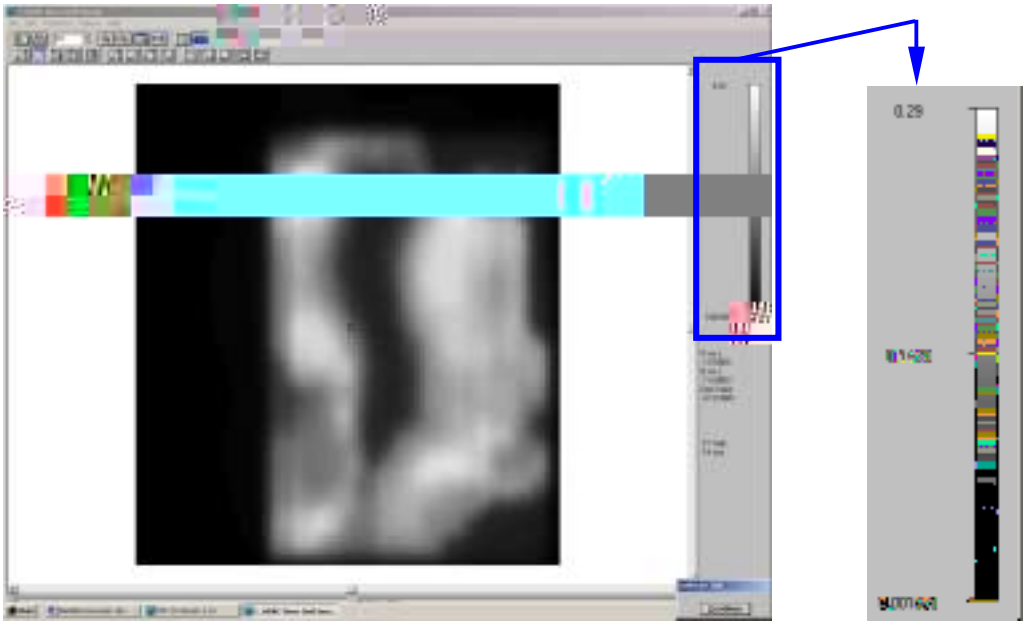

Figure 12. Imported plan image file

Table 1. Plan image dose values

RGB value	Dose Rate (cGy/MU)	Dose (cGy)
0	0.001681	0.309304
127.5	0.1459	26.8456
255	0.29	53.36

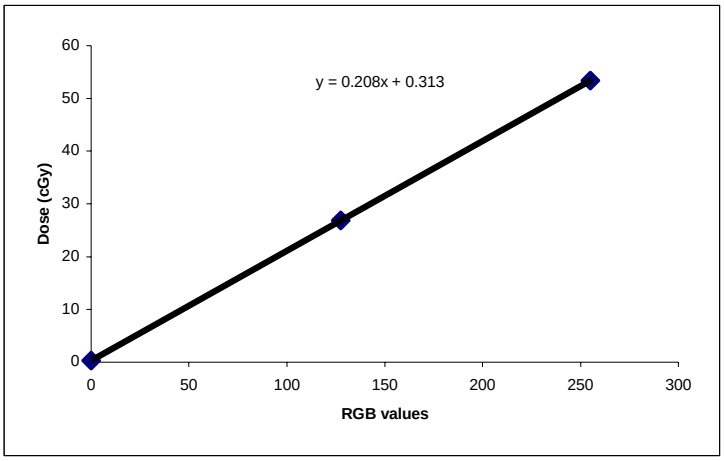

Figure 13. Plan image calibration curve

In retrospect, since the relationship is linear and the plan data values are exact, MS Excel was not needed. All that was needed was to record the minimum and maximum dose values from which we could calculate the slope and intercept directly as

Eq. 2. $$slope = \frac{\max dose - \min dose}{255 - 0}; \quad intercept = \min dose$$

Conversion of Plan Image Files to TIFF Format

After obtaining the data for the plan calibration, the RIT113 software was used to export the plan images as TIFF files. Together, the TIFF files and the plan calibrations are used to import the TPS plan into our IMRT analysis software.

CR Plate Calibration and Conversion

CR Plate Calibration Curve

CR plate calibration curves for each of the three energies used were acquired by exposing several plates to a series of doses using 5 x 5 cm^2 field sizes, 100 cm SPD and 95 cm SSD.

First we exposed a set of plates by doing both one exposure per plate and several exposures per plate for all of the three energies used; Figure 14 shows sample images from these exRTmage35.8(2e)1.re wob a v usehaport t[(er plavalu.2(doows)notows)chanimage

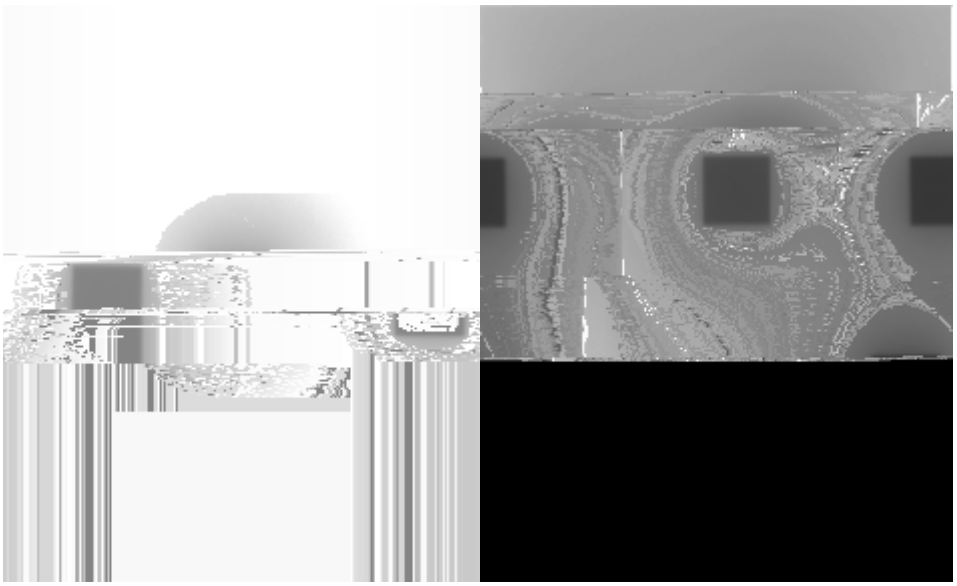

Figure 14. Example CR plate calibration images showing a single field per plate (left) and multiple fields per plate (right)

Eq. 3. $$D = MU \cdot S_{c,p}(5x5) \cdot TMR(5,5) \cdot \left(\frac{100cm + d_m}{100cm}\right)^2$$

Knowing the depth of the point of interest (5 cm), the depth of maximum dose d_m (cm), field size used (5 x 5 cm^2) and the corresponding $S_{c,p}$ and TMR, and

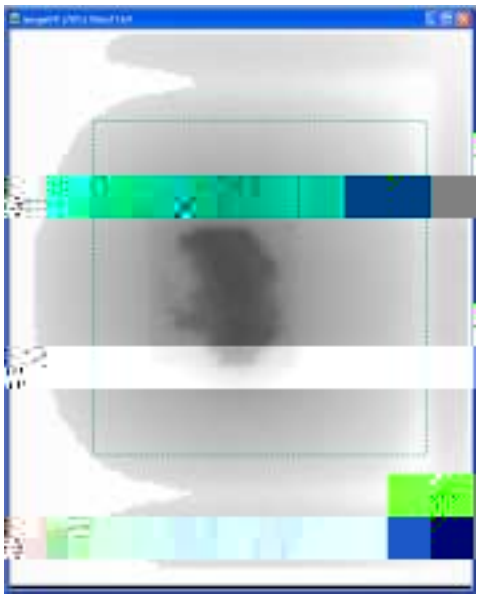

Figure 15. Plate image cropping

The plan images must be resized too. The plan images were resized by the same percentage value (700%) and cropped to 700 x 700 pixels. Now both images are comparable in size and ready for the analysis, except that the two images are probably not aligned. The plate and plan images may not have the exposed area located at the same position. They may be rotated and/or shifted relative to each other. The automatic image registration algorithm (described in the next section) aligns the plate image to the reference plan image.

Image Registration

To accurately compare plan and plate images, by comparing absolute dose values at different points in the field as well as horizontal and vertical dose profiles ,

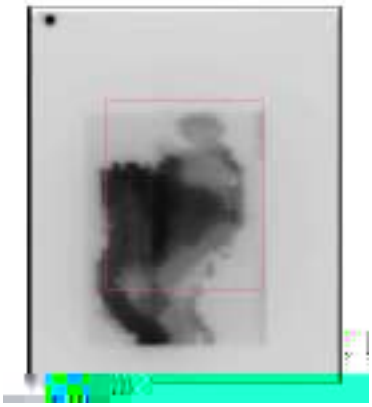

Figure 16. Image cropping

For its image registration method the RIT software uses control-points. With control points, the target image is registered into the image space of a reference image. A set of control points are defined in both images (Figure 17). Comparison of the control point locations identifies necessary rotation, scaling and shift. An affine transform then corrects the target image to align to the reference image.[16]

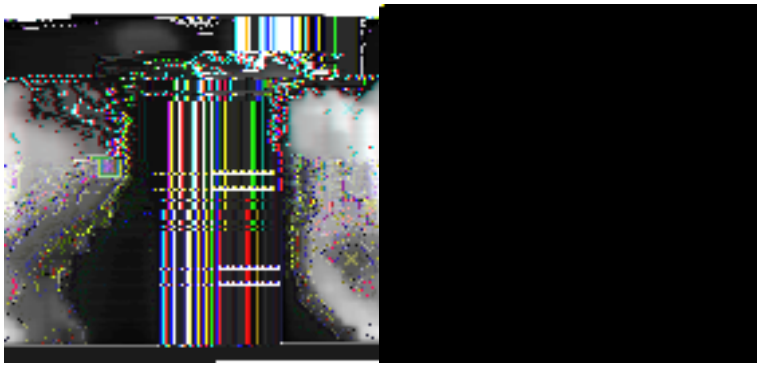

Figure 17. Control points placement in RIT113 v3.14

Ideally, the manually placed control points mark identical places in the target

subjective. If control points are not placed carefully and accurately, very different results may be obtained as demonstrated in Figure 18.

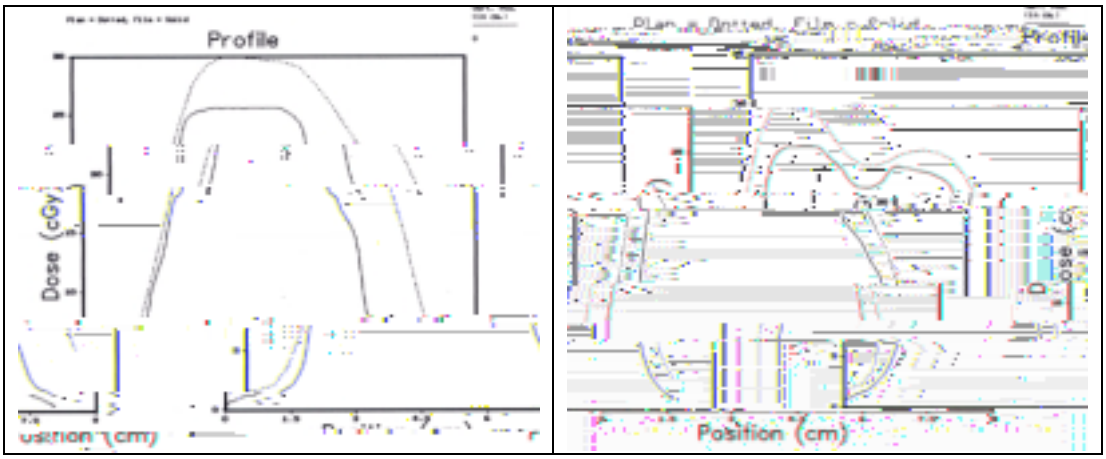

1st user

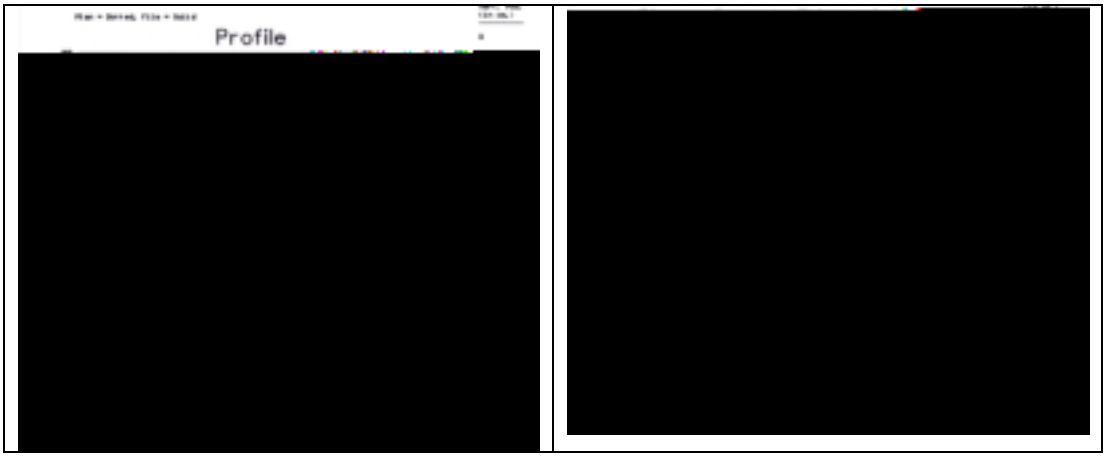

2nd user

Figure 18. Profiles depending on the control points placement and cropping

The quality of analysis strongly depends on the operator and may not be accurate or reproducible. The profiles shown in Figure 18 were generated from registered images where the control points were set by two different users; although

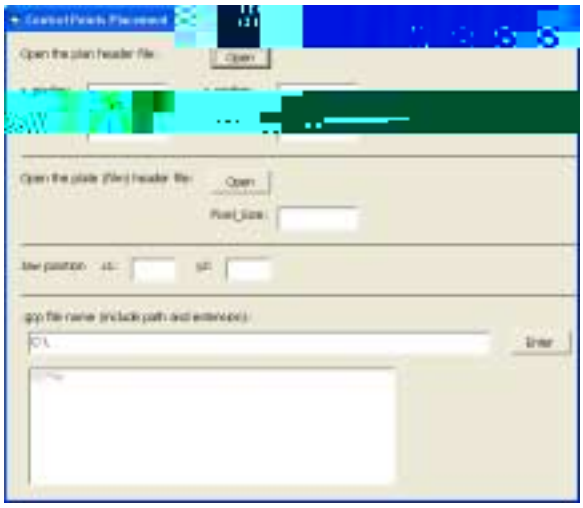

Figure 19. Graphical user interface
(for the automatic creation of the RIT system .gcp file)

Mathematics running in the background of the program uses x1 and y2 jaw positions that can be obtained from the plan printout sheet and pixel dimensions from both header files, as well as x and y start positions from the plan header file, for the calculation of the control points location.

Knowing that x1 and y2 jaw positions represent the origin, the calculation was done as follows:

$$x_{plan} = \frac{|x_{start}| + x_i}{PixelSize} \qquad y_{plan} = \frac{|y_{start}| + y_i}{PixelSize}$$

$$\_\_\_\_\_ \qquad \frac{y \quad y}{PixelSize}$$

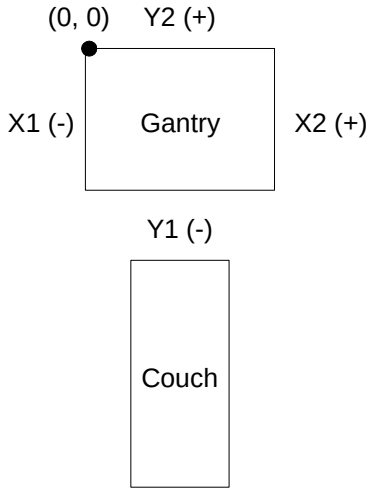

Figure 20. Jaws

What is actually calculated is how many pixels in both x and y direction from the origin control points are located. The origin on a plan image is represented by x_{start} and y_{start} values that are read from the plan image header file as given by the TPS. The same origin on the plate image is given by the position of the x1 and y2 jaws. Since both images also have different pixel sizes, that are again obtained from their header files, values calculated for x_{plan}, y_{plan}, x_{plate} and y_{plate} will be different. Points x_i and y_i are, at present time, picked by the program from a built-in array, that records the smallest possible field size values. The program can be easily changed to allow the user to select the four (or as many as necessary) arbitrary points. Since it is much faster to have points predefined in the program (instead of the user entering them manually) the decision was made to have predefined points in

the program. Once control point locations are calculated they are written into the RIT113 .gcp file format, so that the RIT system can load and use them.

The first step in using this program is to open the plan header file; in the next step, the plate (or film) header file is opened. Values needed for the program execution are automatically populated into the appropriate text boxes; x1 and y2 jaw positions need to be manually entered. Once desired location and name of the .gcp file is entered in the designated text box, by clicking on the 'Enter' button, the .gcp file is automatically created and control point locations are displayed in the text box inside the program itself. The program places four arbitrary points on both (plan and plate or film) image files, as explained previously.

Once finished, the .gcp file now can be used in the RIT113 software for automatic control points placement instead of placing control points manually. By utilizing this program subjectivity of the points placement is gone, i.e. it is not user dependent any more and cases like the one shown in Figure 18 can now be completely eliminated.

This process is useful in the alignment of an acquired image over a template, a time series of images of the same scene, or the separate bands of a composite image (co-registration). One practical application of this process is the alignment of multi-modality images in radiology.

There are several different methods used for image registration:[17]

- Correlation
- Transform Methods (including Fourier and Radon transforms)
- Point Mapping (affine transformation)
- Edge-based methods

Correlation based techniques use a 2D normalized correlation function that measures the similarity for each translation in an image patch, but the data must be normalized to avoid contributions from local image intensities.

Fourier transform based techniques use the correlation theorem: the Fourier transform of the correlation of two images is the product of the Fourier transform of one image and the complex conjugate of the Fourier transform of the other. These techniques use several different approaches: phase-correlation, cross power spectrum, etc.Point mapping techniques use control points, point mapping with feedback, or a global polynomial approach for the image registration. Control points can be intrinsic (markers used within image) or extrinsic (control points automatically or manually selected). After the selection of the control points different methods can be used for the registration of the sets of control points (this

method is used by the RIT113 software). Point mapping with feedback determines the optimal spatial transformation between images by an evaluation of all possible pairs of feature matches.[17] This method can use intensities more or less directly for the image registration. It compares intensities between a transformed version of the image and the fixed (reference) image, utilizes pixel by pixel evaluation within the region, and then applies inverse mapping at each pixel. This can create problems in the sense that inverse mapping of a pixel may not 'land' on a discrete pixel location. In that case interpolation is used: nearest neighbor, bilinear or trilinear (in 3D), spline or sinc. Global polynomial transformation uses a set of matched points to generate a single optimal transformation.

In edge-based techniques, edge-enhanced images (generated from the reference and destination images) are processed to extract straight line segments, which are then grouped to form triangles. A set of candidate transformations is determined by matching triangles from the reference and destination images. The transformations are evaluated by matching the transformed set of reference (source) segments to the set of destination segments.[18] For typical image registration problems, the sources of differences between two images fall into the following categories:

- Differences of alignment between images are caused by a spatial mapping from one image to the other. Typical mappings involve translation, rotation,

warping, and scaling. Changing the orientation or parameters of the imaging sensor can cause differences of alignment.

- Differences from occlusion (one object partially hidden by another) occur when part of a finite image moves out of the image frame or new data enters the image frame of a finite image due to an alignment difference, or to an obstruction coming between the imaging sensor and the object being imaged.
- Differences from noise occur from sampling error and background noise in the sensor, and from unidentifiably invalid data introduced by sensor error.
- Differences due to change are actual differences between the objects or scenes being imaged. It may be impossible to distinguish between change and noise.

Most often, images are registered to facilitate detecting the changes in a scene; successful registration detects and undoes (or accounts for) differences due to alignment, occlusion, and noise while preserving difference due to change. Registration algorithms must assume that change is small with respect to the content of the image; that is, the images being registered are assumed to be “visibly similar" after accounting for differences due to alignment, occlusion, and noise. In addition, a sufficient amount of the object or scene must be commonly visible in both images. Often, algorithms require that at least 50% of the content of the reference image also

The corresponding Fourier transforms $I1(u,v)$ and $I2(u,v)$ are related by

Eq. 7. $$I2(u,v) = e^{-i\phi_{i2}(u,v)}\sigma^{-2}\left|I1\left(\sigma^{-1}[u\cos\alpha + v\sin\alpha], \sigma^{-1}[-u\sin\alpha + v\cos\alpha]\right)\right|$$

where $\phi_{i2}(u,v)$ is the frequency phase of the image $i2(x,y)$. $\phi_{i2}(u,v)$ depends on the translation, rotation and scaling, but the frequency magnitude

- Filtered FFT-ed magnitudes of both images are transformed from Cartesian to log-polar coordinates
- FFT is applied to the log-polar data
- Ratio of the two FFT-ed log-polar images is computed
- Inverse FFT of the ratio is calculated
- Absolute value of the inverse FFT of the ratio is computed
-

using the bony structures (spine for example)); in portal imaging for patient positioning assessment; etc. The easiest implementation may be in tomotherapy since

calibrated and cropped, the same point on the film is selected. The value at this point is compared to the value obtained from the plan. The two values should agree within 5%. In the second step, plan and film images are registered and vertical and horizontal profiles are compared (the profiles are usually chosen to go through the maximum dose point). Profiles are usually reported in absolute dose. As a last step, film isodose lines are generated (also in absolute dose).

On the other hand diode arrays like MapCheck compare normalized values (normalized to a 'best fit' point) and display points (diodes) that do not fall within criteria (3% and 3 mm DTA – distance to agreement). In this case isodose lines and profiles are normalized. The point used for both absolute dose comparison and normalization is chosen from the area where maximum dose is delivered (a low gradient and low modulation area).

We followed these common practices when our program for IMRT analysis was developed. The same rules were applied as for film: the point for absolute dose comparison is the maximum dose read on plan and plate images, the position of the maximum point is read and displayed, two vertical and two horizontal profiles are read and compared, both normalized and absolute isodose lines are displayed for both plan and plate, and the intensity map for both images is displayed (in 2D and 3D). The results are described in the next chapter.

Results and Discussion

When the study started, a different model of CR plate was used other than the one that the study was finally finished with (Agfa MD10). The plates used at the start were thicker and cracked easily, and that was the main reason why Kodak replaced them. Plate particles would quickly mess up the rollers in the scanner so it had to be cleaned often; consequently portal images were of very bad quality. In Figure 22 two white lines are clearly visible; they are the result of plate debris that fell into the scanner and stuck to the rollers. If the lines and other artifacts were in the exposed area, accurate analysis (dosimetry) would not be possible. In this paper, the original set of plates will be referred to as 'old' and the Agfa MD10 plates used later on as 'new'. For all the tests, plates were randomly selected; we didn't just use one plate over again. This was done mainly because the goal of the study was to explore the possibility of CR plates being good replacements for film dosimetry. Also, if only one plate was used for all the measurements, a considerable amount of time would be lost just waiting for that plate to be erased each time. As one sees hereafter, the plates all show similar (one can even say same) behavior.

Several different tests were done throughout the course of the study. All the exposures with the old plates were done with 4 MV only; exposures with all energies were made with the new plates. After the first few exposures of the study were done,

the Kodak scanner was serviced. The values read on the plates changed considerably after the service.

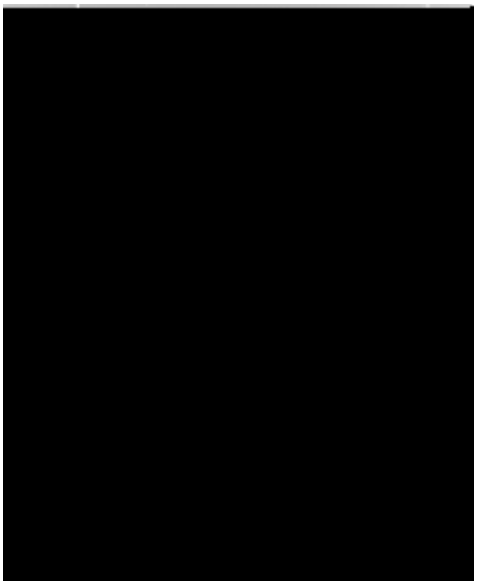

Figure 22. CR plate image

Lead vs. No Lead Plate Exposure

Several exposures were done using lead sheets ranging from 1 mm to 10 mm thick; we then repeated the exposures with the same number of monitor units delivered but without the lead. Table 3 shows results for 1 mm lead vs. no lead. It can be noticed that even though the absolute difference between values read is comparable for all MU delivered, the relative percentage difference increases with higher numbers of MU delivered because of the smaller magnitude of the RGB

values. Due to issues related to handling of the plates with lead sheets while doing hundreds of exposures (time consuming and contamination is a possibility), it was decided to continue with the exposures without using the lead. Exposures with lead were done only with 4 MV, and different lead thicknesses used gave similar results to those presented in Table 3.

Table 3. Exposure with lead vs. without (4 MV) – 'old' plates used

	RGB values read in center of 5 x 5 area		
MU	**1 mm lead**	**no lead**	**% difference**
5	79	76	3.9
10	50	48	4.2
15	32	33	-3.0
20	20	22	-9.0
25	10	11	-9.0
30	0	0	0.0

Multiple Exposures vs. One Exposure Per Plate

Exposures on different days with the same number of monitor units were done to be able to establish if one calibration curve will be enough for all plates. Measurements were repeated both for one exposure per one plate and for multiple exposures per plate with the same number of monitor units. Figure 23 shows sample images.

Delivering a higher dose (more monitor units) results in darker values. The values read showed little difference (all differences were less than 2%); Table 4 presents part of the data that is representative of the obtained values.

Cassette vs. No Cassette Exposure

Exposures were also repeated for several monitor units with and without the cassette, with typical results shown in Table 5. Again due to handling issues (cassettes are heavy and hard to manipulate), and because the presence of the cassette does not make considerable difference in the result, plates without the

Table 6. Decay analysis

	RGB value			
MU	Scanned 5 min after x-ray exposure (before scan plate was exposed to bright flash light)	Scanned immediately	Scanned after 10 min	3 min bright flash light exposure
30	1	80	83	40
	Scanned immediately	Plate exposed on reverse side and scanned immediately		
5	130	2		

It is obvious that by exposing the irradiated plate to bright light (a flash light was used) the plates become overexposed. For example if plate was scanned immediately after exposure or 10 minutes after it was exposed to same number of MUs (30), the values read were almost the same. But if the plate was exposed to 30 MUs and then before scanning taken out of envelope and flashed with a bright light, the results read after the scanning of these plates changed considerably. This actually shows why Kodak does recommend for plates to be read and used in areas with dim light. One of the plates that was exposed to 5 MUs was exposed backwards, i.e. the white side of the plate was not facing the x-ray source, but rather its back. The plate was scanned normally. We wanted to see what would be the result if someone turned a plate upside down unintentionally and exposed it that way.

Further Analysis of the Plate Behavior

Table 8. Percentage difference range

MU	RGB value range	% difference
5	121 - 124	2.4
10	104 - 107	2.8
15	97 – 99	2.0
20	89 - 90	1.1
25	82 - 83	1.2
30	77 - 78	1.3
40	72 - 73	1.4
60	60 - 61	1.6

Table 9. Erasure time dependence

MU	**Plate number**				
	2	**3**	**4**	**5**	**6**
5	81	122	81	122	123
10	60	107	59	106	106
20	38	90	37	90	89
40	16	73	16	73	73
60	2	61	2	61	61

Before the study was done to obtain the results shown in Table 9, first the plate was erased (#1) and then exposed. The rest of the plates were handled as follows:

- #2 – taken from previously cleaned plate (#1)
- #3 – was taken from scanner immediately after erasure
- #4 – was taken out 5 min after erasure finished
- #5 - was taken out 10 min after erasure finished
- #6 – was taken out immediately

available (assuming Gaussian statistics). Thus the results shown in Table 8 represent reproducibility of the plates and show that it is on the order of 2%.

Excluding the ‘random behavior’, the plates performed consistently from day to day and exposure to exposure. Thus we concluded that one calibration curve could be used all the time. There is no need to do separate calibration curves every time IMRT QA is performed, as it is done now in film dosimetry. Appendix G provides the results of a separate study that shows the large variations in calibration values encountered in film dosimetry, depending on when the exposures are done.

This study of erasure time dependence was done only for the ‘old’ plates and it was not repeated for the ‘new’ ones. Both ‘old’ and ‘new’ plates exhibited the ‘random overexposure’ behavior.

IMRT Analysis

Using ‘Old’ Plates

In the first IMRT exposures (done with ‘old’ plates), we tried to follow the film dosimetry procedure. At first, the RIT113 system was used, but it had problems with reading Kodak DICOM images, as discussed previously. Also the calibration curve results did not look very promising; Figure 24 compares film and plate calibration curves determined with the RIT113 software. Figure 25 shows the calibration plate image for 20, 40, 60 and 80 MU.

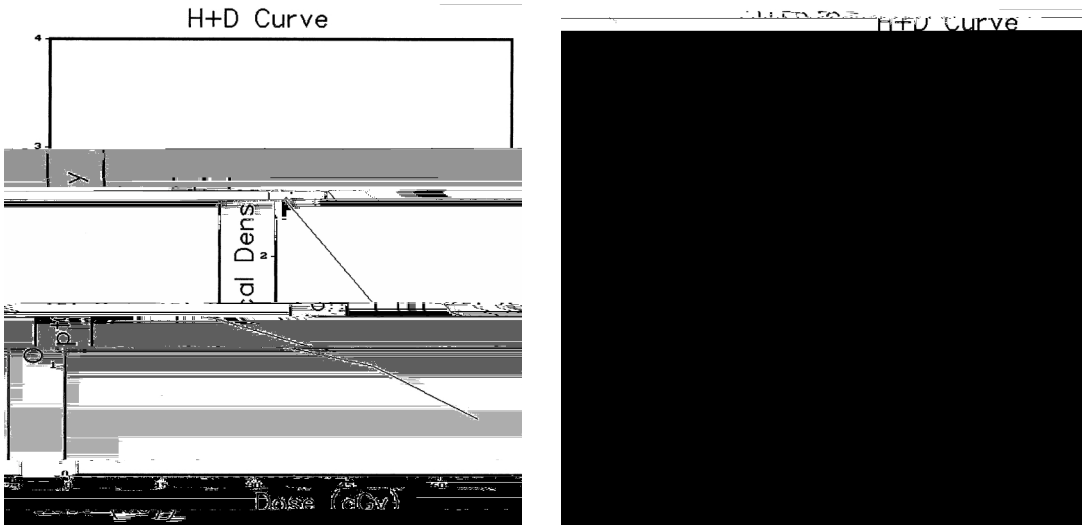

PLATE FILM

Figure 24. Example of calibration curve done with RIT113 v. 3.14

After the IMRT analysis algorithm was developed, the analysis for the plate image in Figure 25 was repeated. Figure 26 shows the calibration curve that was generated and used in the analysis. Using the plan calibration curve shown in Figure 13, an 'old' plate was used to deliver one patient IMRT QA plan. The resulting plate image, a dose profile, and isodose contours are shown in Figure 27 for one of the delivered fields.

It is obvious that four points for the calibration curve are not enough to accurately represent all the values on the plate image; a curve with more measured points is needed.

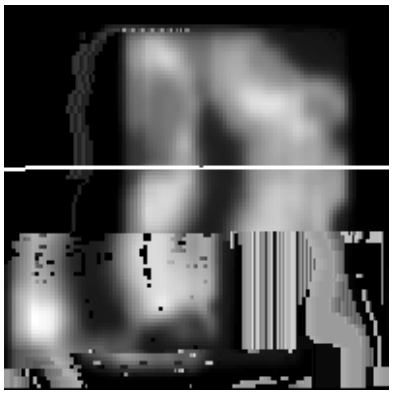

Profile Location

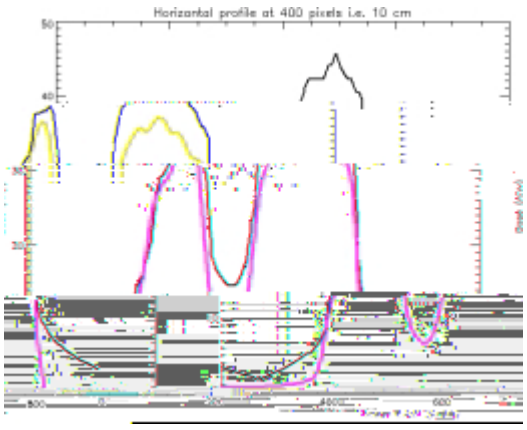

Profile, plan is blue

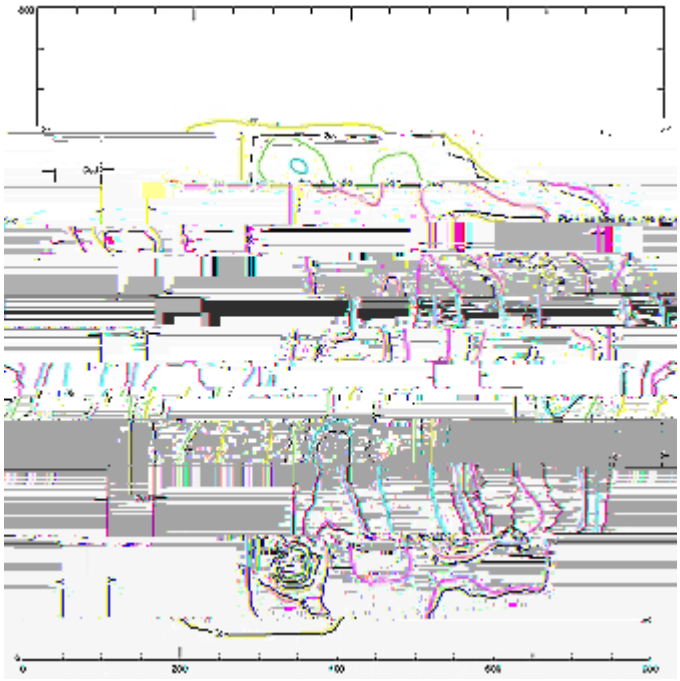

Isodose Lines (in %)

Maximum value in Plan array is: 53.3530
The maximum value of Plan is at location (18, 828)

Maximum value in Plate array is: 59.3139
The maximum value of Plate is at location (18, 828)

Percentage difference: 11%

Figure 27. First results

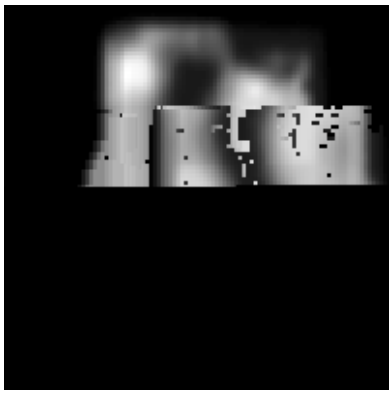

Profile Location

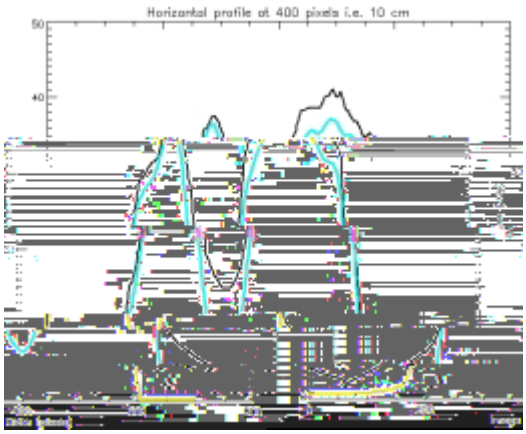

Profile, plan is blue

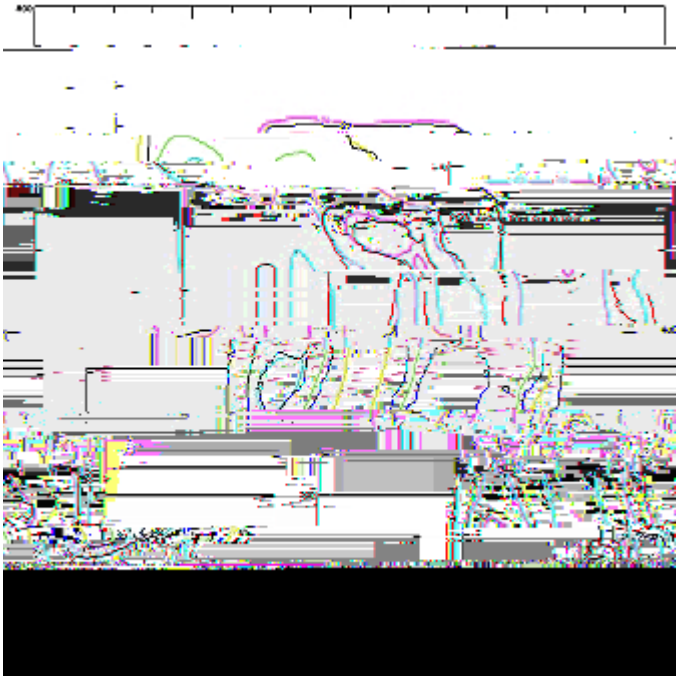

Isodose Lines (in %)

It may be noticed that for the ranges given in Table 8, the values reported in Table 10 fall outside that range. The exposures and measurements done for this patient plan were done after plates were cleaned with the Kodak-recommended solution. After this cleaning, we did not repeat exposures to establish a range of values like the ones reported in Table 8.

From the figures, it is obvious that a curve with more points gives better results if only profiles are compared. Unfortunately further analysis with this kind of plate was not possible because they were soon replaced with the Agfa MD10 plates and rest of the study was done using those plates.

Using 'New' Plates

Calibration Curves Used

The data used for the generation of the calibration curves shown in this section are presented in Appendix H. Calibration curves data were obtained in 1 MU intervals, using both single and multiple exposures per plate; exposures were done on different days.

An exponential trend of values from the plate images was observed. Each data set in Appendix H was graphed in MS Excel and an exponential function was

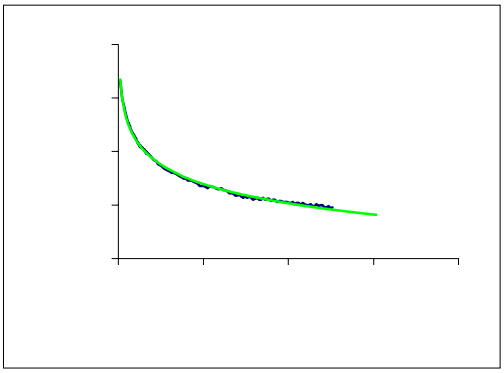

the differences will be practically invisible. As expected in most cases, the curve with the most calibration points gave best results. So in practice only the full calibration curve should be used. On the figures below where 0% is indicated, it means that the percentage difference between the two values was less than 0.5%.

4 MV, with the fewer points (up to 80 MU) calibration curve	**4 MV, with the maximum points (up to 130 MU) calibration curve**

6 MV, with the fewer points (up to 70 MU) calibration curve	6 MV, with the maximum points (up to 135 MU) calibration curve
Maximum value in Plan array is: 69.2648 The maximum value of Plan is at location (2, 2377) Maximum value in Plate array is: 63.2072 The maximum value of Plate is at location (14, 2132) Percentage difference: -9%	Maximum value in Plan array is: 69.2648 The maximum value of Plan is at location (2, 2377) Maximum value in Plate array is: 69.1400 The maximum value of Plate is at location (14, 2132) Percentage difference: 0%
	
Normalized isodose lines, plan values are in color	
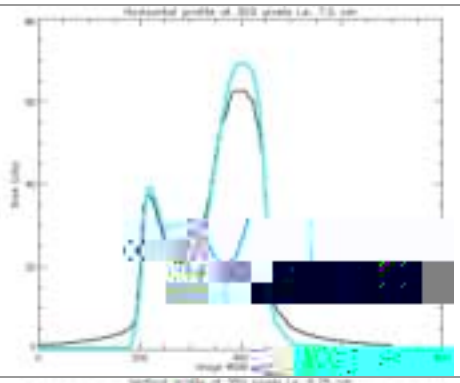	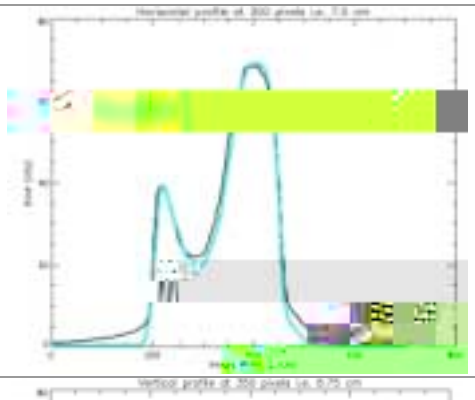
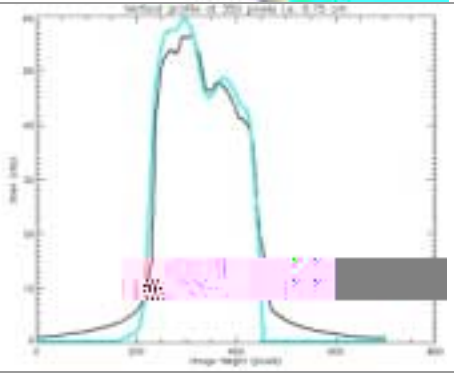	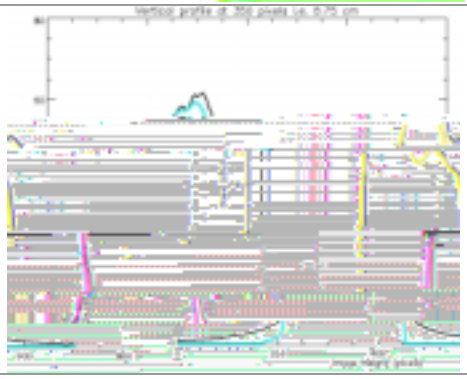

Figure 34. Comparison based on calibration curves used (6 MV)

IMRT Analysis – Output of the Algorithm Developed

TIFF format for both plan and plate images is used as the input to the developed algorithm together with the values for the corresponding calibration curves. Typical output generated after the program runs is shown in the images below.

(*Note:* For the first field some of the windows that are created as the output are left in their original background color – black, while for the second case the window's color is inverted to make the results more visible on paper.)

6 MV

1st field

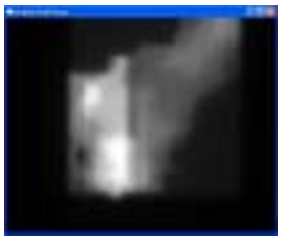

Original plan image

Original plate image

Converted plan image

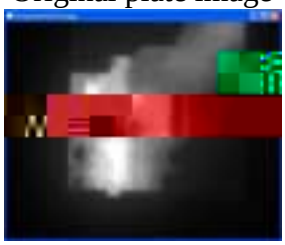

Converted plate image

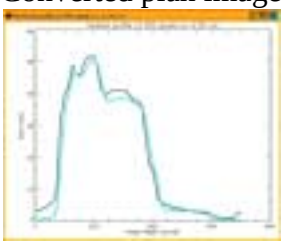

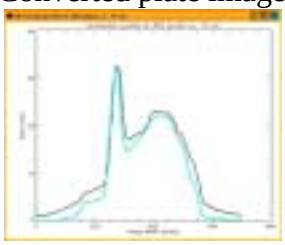

1st vertical profile

1st horizontal profile

1st field

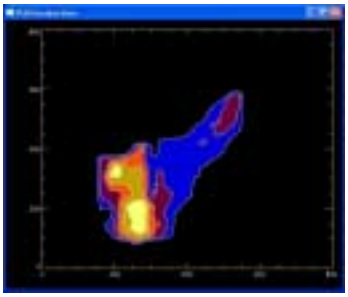

Plan isodose lines in absolute dose

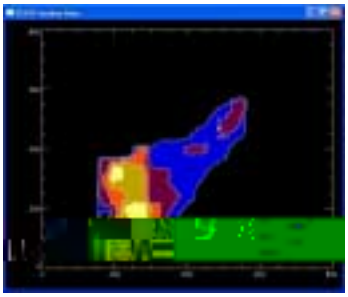

Plate isodose lines in absolute dose

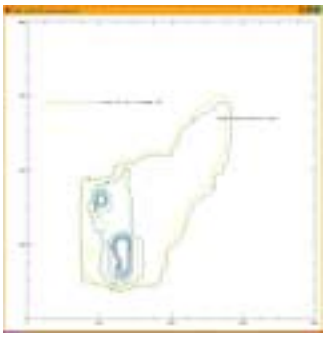

Plan and plate normalized isodose lines(normalization is done using maximum value read)

Maximum value in Plan array is: 51.6569
The maximum value of Plan is at location (63, 1269)

Maximum value in Plate array is: 51.8616
The maximum value of Plate is at location (63, 982)

Percentage difference: 0%

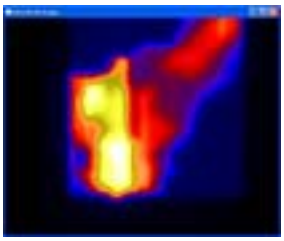

Plan fluence map

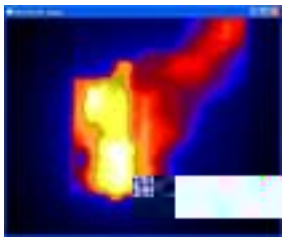

Plate fluence map

2nd field

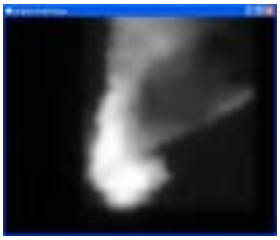

Original plan image

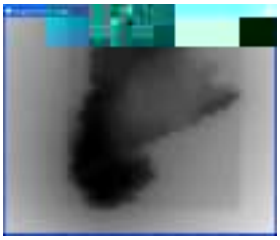

Original plate image

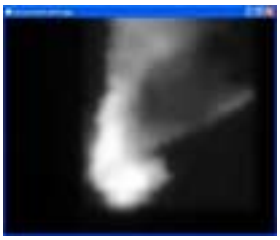

Converted plan image

Converted plate image

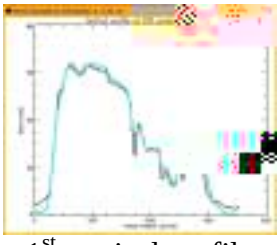

1st vertical profile

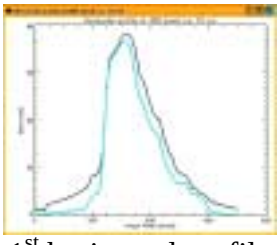

1st horizontal profile

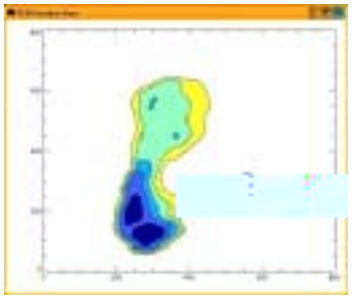

Plan isodose lines in absolute dose

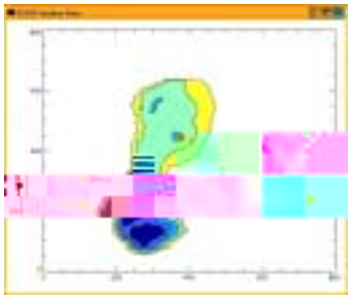

Plate isodose lines in absolute dose

2nd field

Plan and plate normalized isodose lines
(normalization is done using maximum value read)

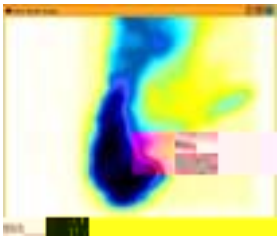

Plan fluence map

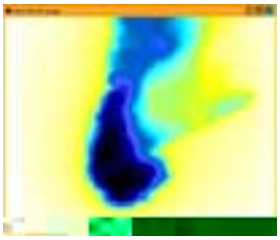

Plate fluence map

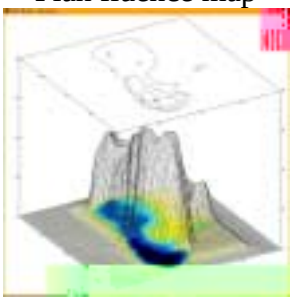

Plan 3D intensity profile

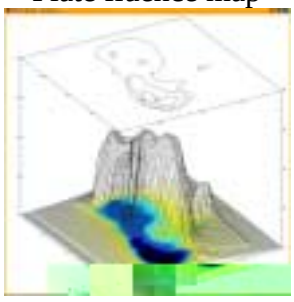

Plate 3D intensity profile

Maximum value in Plan array is: 64.1980
The maximum value of Plan is at location (85, 842)

Maximum value in Plate array is: 63.1858
The maximum value of Plate is at location (71, 646)

Percentage difference: -2%

The 6 MV plates showed the best behavior compared to the profiles generated with different patient plans with different energies, and percentage

differences in maximum absolute dose values read for all fields delivered were between –2% and 4%. The 4 MV plate behaved inferiorly when the absolute maximum dose values were compared in comparison to the other two energies. Percentage difference for all fields was within –10% to 2%, even though normalized isodose lines were a perfect match (this is the way values are checked in MapCheck for example, while for absolute dose value comparison, best values are found and often chosen purposely for reporting!). For 10 MV, same as for 4 MV, plates were usually underexposed, but the differences in maximum absolute doses were still within –8% to 0%. One reason could be the calibration curve; if a better choice of calibration curve was made the results might be better. One way of dealing with the obvious disagreements between the profiles in low dose regions is to chose a separate calibration curve for that particular range of values; another way would be by placing lead sheets on both sides of the plate (as it is done sometimes with film) to filter low-energy photons. As shown previously results were not significantly different with lead, but still for lower dose values, they were different enough to matter. And above all the same test was not done for the ‘new’ plates.

Contrary to 4 MV and 6 MV, the 10 MV plate was usually underexposed in higher dose regions and had better matching with planned values in lower dose regions.

Even though percentage differences for some fields seem to be quite high, higher differences are observed sometimes with film dosimetry and either neglected

if all other parameters are within acceptable limits or the exposure is repeated. There is not much sense in repeating plate exposures since its response doesn't change from day to day, although it can certainly change in relation to accidental exposure to bright light or its own 'random behavior'. Time decay of the plate data was not significant in the time frame we used for scanning each exposed plate, but it must be considered if plates are not scanned immediately after exposure.

Many of the fields had to be repeated, as they were overexposed (Figure 35). Table 11 summarizes the fractions of plate exposures that exhibited the 'random overexposure' behavior. Figure 35 compares a properly exposed plate to an overexposed plate for the same field. 6 MV IMRT fields had the lowest number of overexposed images; some patient plans were completely delivered without overexposures, even though 6 MV had the highest number of overexposed images when exposure for calibration curves was done.

The overall percentage of overexposed fields is 23.4%, meaning that roughly 23 plates will be overexposed for 100 images taken. If an average patient plan has 7 fields that must be exposed for IMRT QA, on average ~ 2 fields out of 7 must be repeated. This inexplicable behavior of the plates adversely impacts the time saving advantage that plates have in comparison to film dosimetry.

Table 11. Percentage of the overexposed fields

4 MV	% overexposed	average (in %)
Calibration Images	25.6	

dual-function calibration curve in the analysis program. This is the main reason why many of the profiles show disagreement in the low dose areas of the fields.

It is obvious that even though results were good when the calibration curve used for the analysis was taken as a best fit to the maximum number of data points measured, some results strongly depended on the range of the curve used (i.e. if an exponential equation based on fewer points described the trend the best). When data points were calculated backward, using the trendline equation, they did not necessarily fall within the measured data range. A more accurate approach would be to assign to each pixel in the acquired plate image an exact measured value. The problem with this is computational time. But after all, the analysis did show that in most cases, the best fit approach (trendline) will do.

Finally, we found that one calibration curve can be used for each energy and the calibration doesn't vary over time. The same is not true for film calibration curves regardless of energy (see Appendix G).

Half vs. Full Number of MUs Delivered

In this part of the study several fields were delivered using both half and the full number of monitor units. A typical case is compared in Figure 36 and Figure 37. A slight difference is observed if the same plate calibration curve was used for the fields delivered with half and the full number of MUs delivered for all energies. On the other hand if different calibration curves were used (selected by the maximum

dose expected for the particular field), there was almost no difference in the values and profiles.

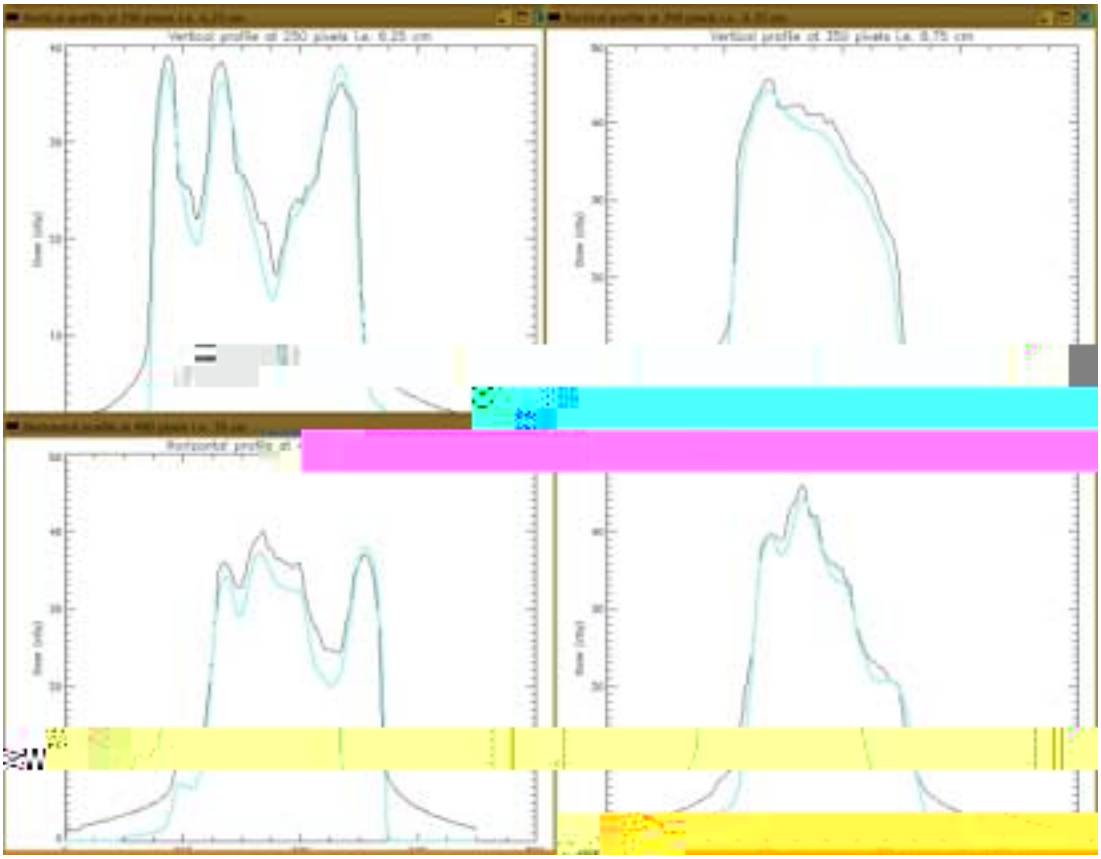

Maximum value in Plan array is: 46.3483
The maximum value of Plan is at location (38, 1928)

Maximum value in Plate array is: 48.6492
The maximum value of Plate is at location (36, 1879)

% difference: 5%

Figure 36. Full number of MUs delivered

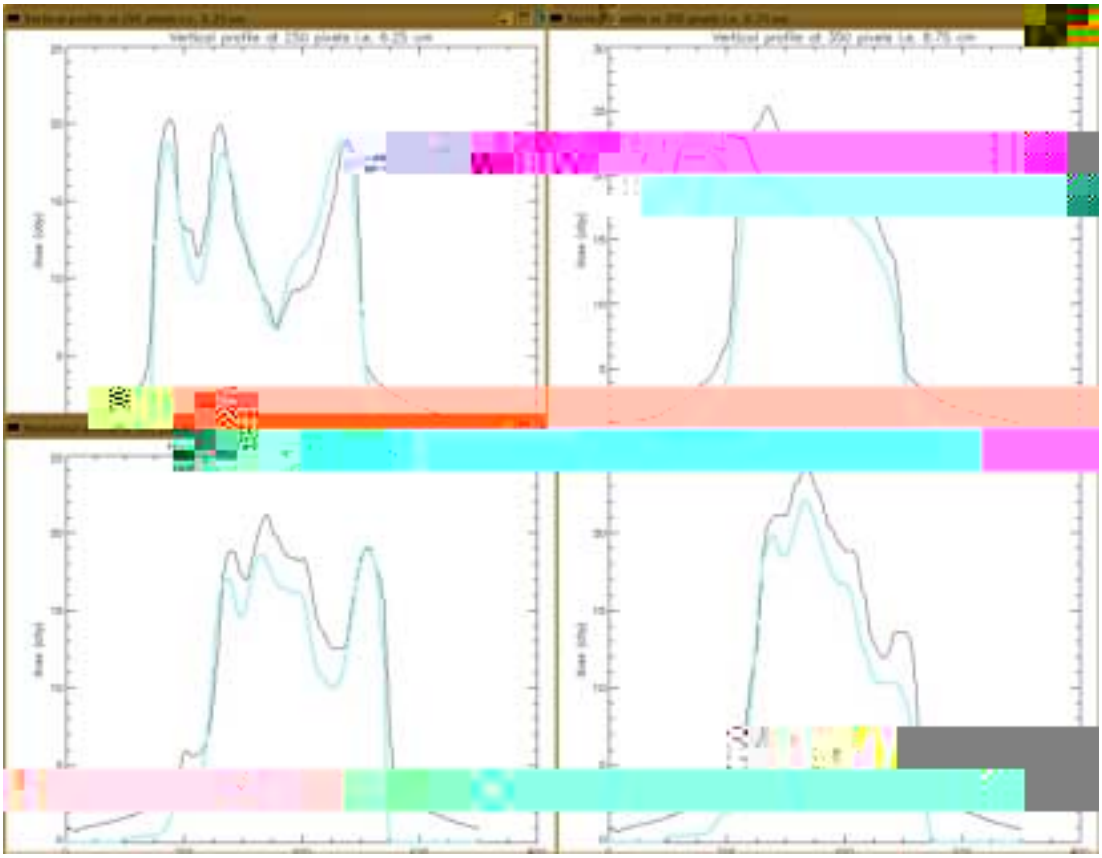

Reproducibility

Typical results for reproducibility are shown in Figure 38 and Figure 39 (plan values are always in color). The case shown as an example in Figure 38 had fields exposed 3 weeks apart.

If the same field was exposed on the same day a couple of times subsequently, maximum value measured on the plate remained the same regardless of the number of exposures done (up to 2% difference was observed in a few cases); a slight difference was observed in the position of the maximum [(8, 2180) instead of (8, 2229) for example].

Surprisingly so, the maximum values measured on a plate for the exposures done 3 weeks apart did not show any difference for this case, but since the same exposure was not repeated again for the same field another 3 weeks apart, no particular conclusions could be drawn.

Original QA session

QA session 3 weeks later

Exposure 1	Exposure 2
Maximum value in Plan array is: 59.9180 The maximum value of Plan is at location (22, 2383) Maximum value in Plate array is: 58.3862 The maximum value of Plate is at location (8, 2180) Percentage difference: -3%	Maximum value in Plan array is: 59.9180 The maximum value of Plan is at location (22, 2383) Maximum value in Plate array is: 58.3862 The maximum value of Plate is at location (8, 2180) Percentage difference: -3%
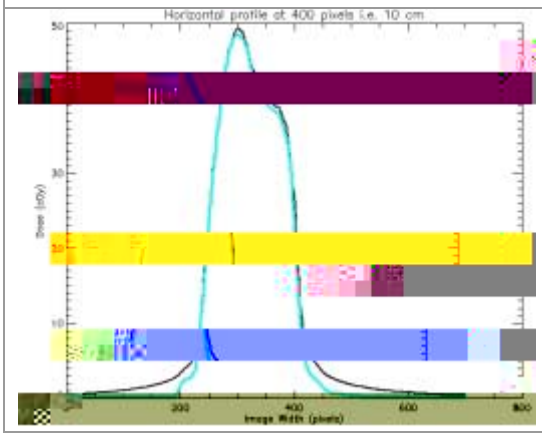	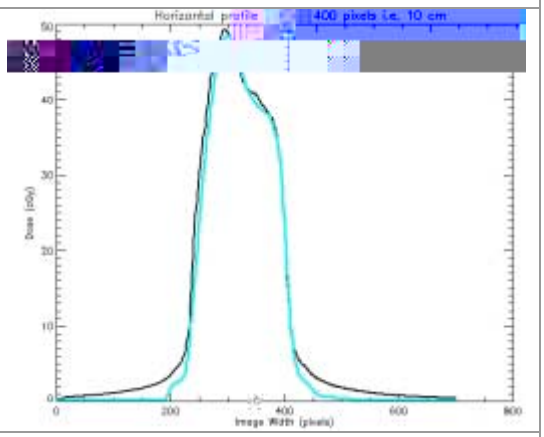
Exposure 3	**Exposure 4**
Maximum value in Plan array is: 59.9180 The maximum value of Plan is at location (22, 2383) Maximum value in Plate array is: 58.7386 The maximum value of Plate is at location (8, 2180) Percentage difference: -2%	Maximum value in Plan array is: 59.9180 The maximum value of Plan is at location (22, 2383) Maximum value in Plate array is: 58.3862 The maximum value of Plate is at location (8, 2229) Percentage difference: -3%
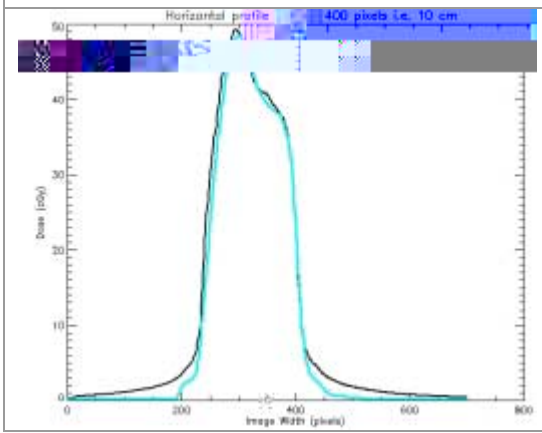	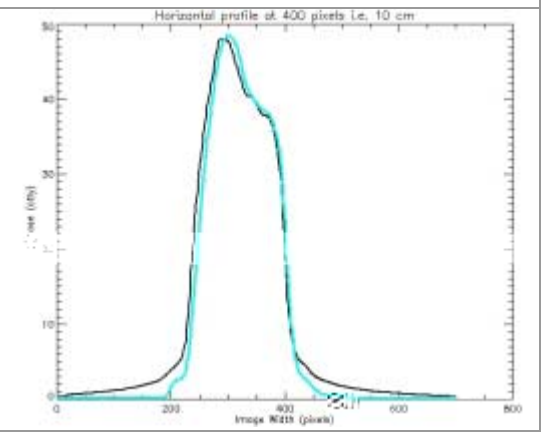

Figure 39. Reproducibility analysis – same day exposure

6 MV

	% difference read for point (absolute dose)
Film	-1.4
Plate	-2

Profiles

Profile Location	Film	Plate
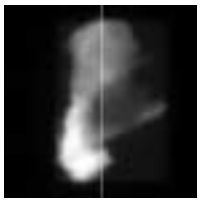	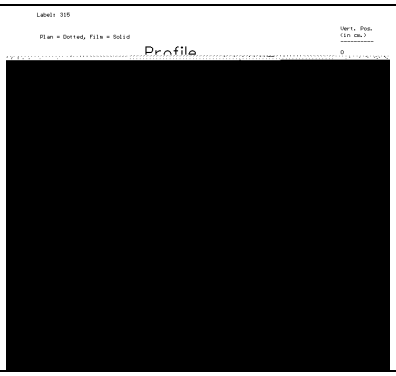	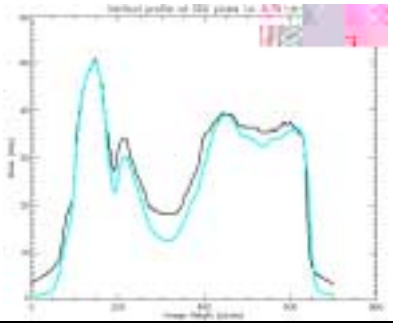
	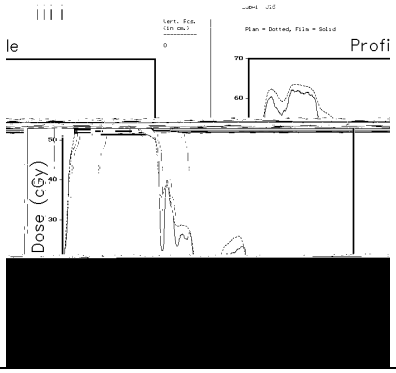	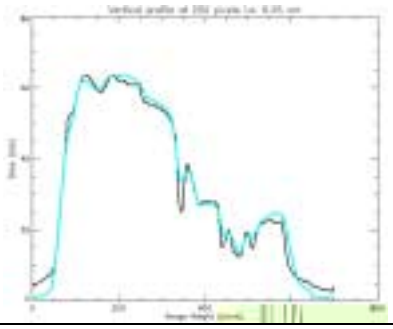
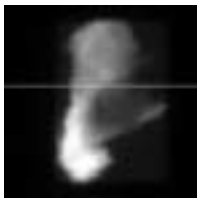	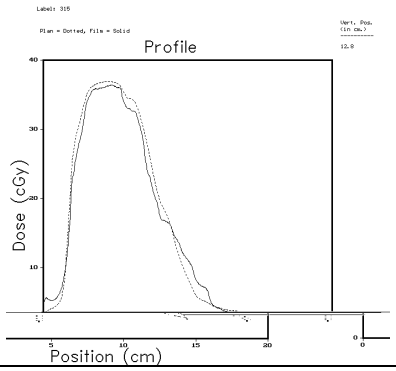	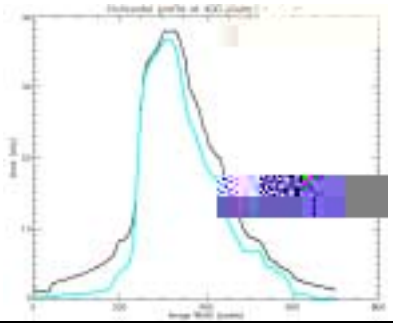

Figure 41. 6 MV, film, plan, plate comparison

10 MV

It should be noted that while both plan and film images are cropped to the same field size, the CR plate image is not, so its value on the field edges does not go artificially to zero. A closer look at the film and plan profiles (especially with 10 MV examples) shows that the film profile is cut off and that the trend of the profile does not necessarily drop to zero at the field edge. In the 10 MV cases, the plate profile follows the plan profile even in the low dose areas (Figure 42).

To have accurate and reliable comparison, the right calibration curve is the most important part. More work should obviously be done in calibration data collection, trying different depths in the phantom (maybe 10 cm which is usually used as the reference depth for calibration purposes for photon beams, where contribution of dose from incident electron contamination is minimal), using different lead sheet thickness, and finding correction factors that will compensate for CR plate and scanner non-uniformities (a Kodak scanner calibration procedure may be needed). Thus by obtaining the most reliable calibration curve decision, the best patient-specific IMRT QA can be made. Overall, it appears that CR plates are a reasonable IMRT QA tool, probably somewhat better than film.

Evaluation of the Automatic Image Registration Algorithm

The registration algorithm was evaluated for several different cases. This evaluation showed some of the algorithm constraints mentioned before:

- if image size is small, rotation is not done right;

- if images are not of the same type, scaling is not done right (evaluation was done using MRI and CT images of the brain);
- otherwise it works fine as one sees on the following figures.

Figure 43 and Figure 44 show the algorithm output for two examples.

Plan image:

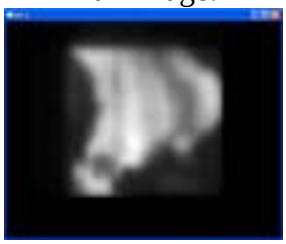

Plate image (before registration):

Plate image (after registration):

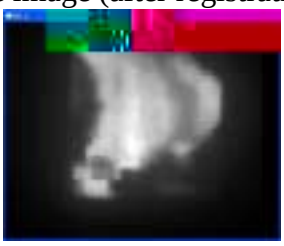

Profiles (y-axis values are in cGy):

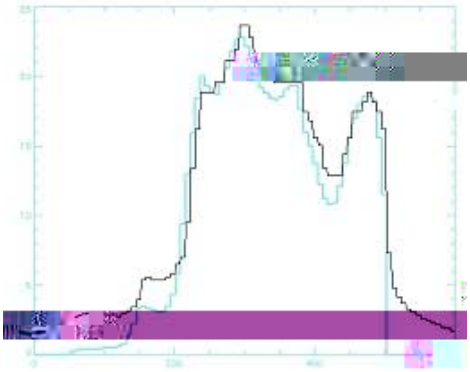

Horizontal

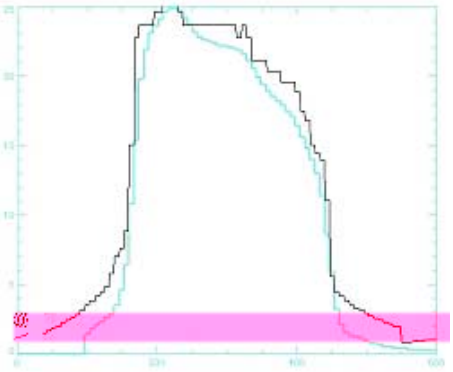

Vertical

Figure 43. Automatic image registration – case I

are in the program used for the IMRT analysis. For the plan and plate images, the registration always appeared to work correctly.

Summary and Conclusions

The purpose of this study was to investigate the possibility of using CR plates instead of film for patient-specific IMRT QA. Several different tests were performed to establish the overall behavior of the CR plates. Overall, 778 exposures were done (calibration and repeated exposures included), from which 609 exposures were done with ‘new’ plates and 169 exposures were done with ‘old’ plates.

Calibration curves were generated for three energies: 4, 6 and 10 MV. It was shown that one curve can be used for each energy independently of the day when the measurement is taken. Saturation of the CR plates and variations in results were noticed for all three energies when more than 100 MU delivered, as it can be seen from the calibration curve deliveries.

It is obvious that even though results were good when the calibration curve

utilize the procedure more efficiently. Finally, CR plate dosimetry has several major advantages over film dosimetry:

- The calibration curve at each energy is stable over time;
- CR plates are less time-consuming than film (using CR plates should be even less time consuming when the analysis process can be automated, the current manual analysis with IDL is faster than film analysis with RIT);
- Working with CR plates is no more difficult than working with film.

In high dose regions, the CR-measured values compare well to planned values. In low dose regions, fields delivered with the full number of MU show better agreement with the plan than fields delivered with half the MU (possibly due to calibration curve limitations at low doses as noted before). One major drawback to CR plates is the inexplicable apparent overexposure of some fields. The specific cause of this behavior could not be identified.

References

1. Faiz M. Khan, The Physics of Radiation Therapy. Lippincott Williams & Wilkins, 3rd edition, (2003).

2. Gary A. Ezzell, Quality Assurance: When and What is Enough for IMRT?. AAPM 2003 Summer School, Intensity-Modulated Radiation Therapy: The State of the Art, (2003).

3. Michael B. Sharpe, Commissioning and Quality Assurance for IMRT Treatment Planning. AAPM 2003 Summer School, Intensity-Modulated Radiation Therapy: The State of the Art, (2003).

4. J. H. Kung, G. T. Y. Chen, F. K. Kuchnir, A monitor unit verification calculation in intensity modulated radiotherapy as a dosimetry quality assurance. Med. Phys. Vol. 27, No 10: 2226-2230, October 2000.

5. ADAC Pinnacle^3, SmartSim User Guide. Version 6.0, August 2001.

6. M. Hareyama, N. Tsuchiya, M. Takebe and T. Chida, Two-dimensional measurement of natural radioactivity of granitic rocks by photostimulated luminescence technique. Geochemical Journal, Vol. 34, 1 - 9, (2000).

7. Heinz Anderle, Physical Methods: Theory. Available online: http://www.anc.univie.ac.at/scripts/anderle_cap4.pdf., 1997. [Downloaded: June 15, 2004]

8. J. A. Seibert, Physics of Computed Radiography. AAPM 1999 Annual Meeting, Nashville, (1999).

9. Kodak 2000RT CR System, Characteristics of a computed radiography system for radiation therapy. Eastman Kodak Company, (2002).

10. Kodak Health Imaging Products by Type, ACR-2000i System. Available online: http://www.kodak.com/global/en/health/productsByType/cr/acr2000i.jhtml. [Downloaded: April 10, 2004].

11. Cardinal Health's Radiation Management Services, Available online: http://www.cardinal.com/rms. [Downloaded: July 3, 2004].

12. Kodak Health Imaging Service and Support, Available online: http://www.kodak.com/global/en/health/serviceAndSupport/dicom.jhtml. [Downloaded: June 25, 2004].

13. DICOM Brahma ActiveX Control, Available online: http://freehost04.websamba.com/dicom4india/dicom_brahma.htm. [Downloaded: April 10, 2004].

14. DICOM plug in, DicomObserver, Available online: http://freehost04.websamba.com/dicom4indiadicom_component.htm. [Downloaded: April 10, 2004].

15. IrfanView, Graphic viewer, Available online: http://www.irfanview.com. [Downloaded: May 11, 2004].

16. RIT113 Film Dosimetry System Version 3.14, User's Manual & Guide. Radiological Imaging Technology, (2002).

17. Image Registration, Image Registration Mapping of Evolution. Available online: http://www.cs.ucsd.edu/classes/fa02/cse252c/Image_Registration.ppt. [Downloaded: May 13, 2004].

18. Enrique Corias, Javier Santamaria, Carlos Miravet, A Segment-based Registration Technique for Visual-IR Images. Available online: http://www.ece.eps.hw.ac.uk/~ecoiras/OptEng_Registration.pdf. [Downloaded: May 15, 2004].

19. UNESCO Training Course, The Frequency Domain. Available online:

23. RSI (Research Systems, Inc.) - Data Analyses and Visualization Software, Removing Noise from an Image with FFT. Available online: http://www.rsinc.com. [Downloaded: May 20, 2004].

24. John P. Gibbons, Monitor Unit Calculations for External Photon and Electron Beams. Advanced Medical Publishing, Inc., (2000).

Appendix A. Varian LINAC 21EX (6-18) Components

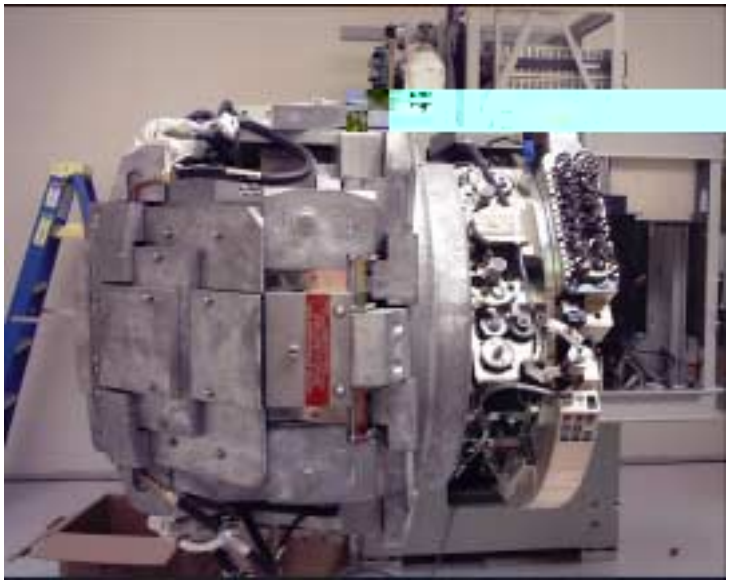

Treatment Head
(shielding blocks, and electro motors used for the MLC control are visible)

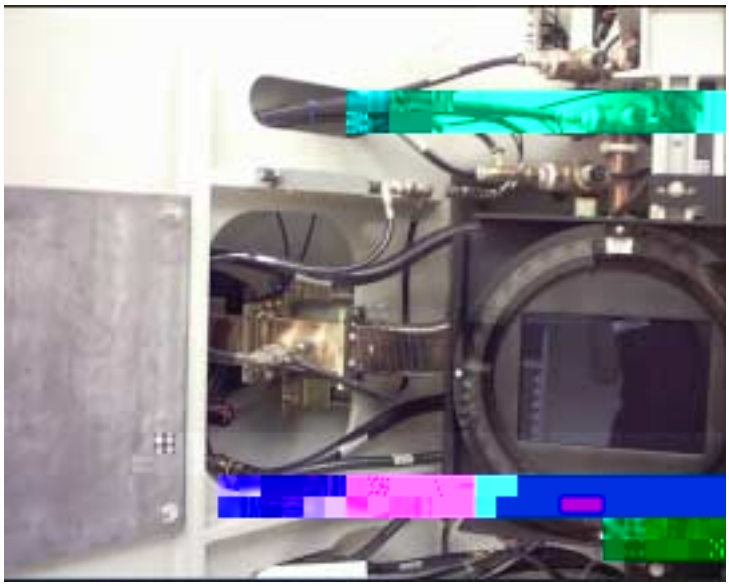

RF power coming from Klystron (Wave Guide System)

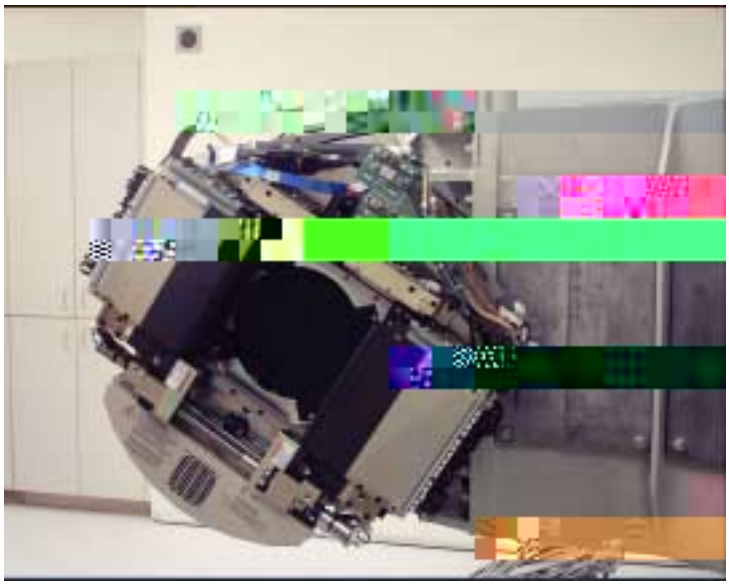

View of the Collimators (Jaws) and MLCs in the Treatment Head

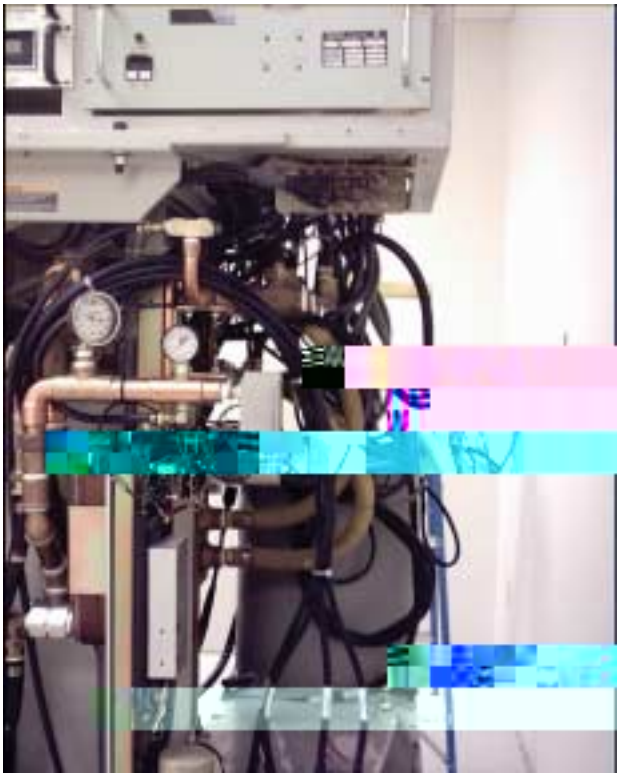

LINAC's ancillary equipment
(Klystron is visible behind the cables)

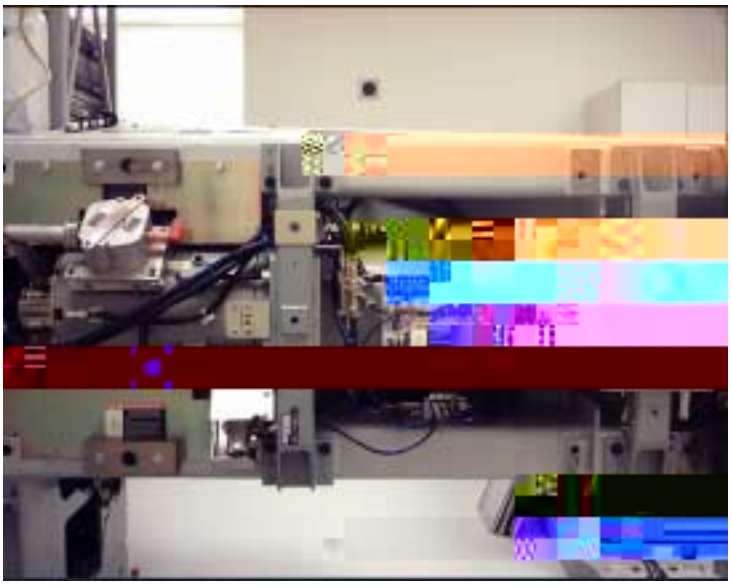

Accelerator Tube

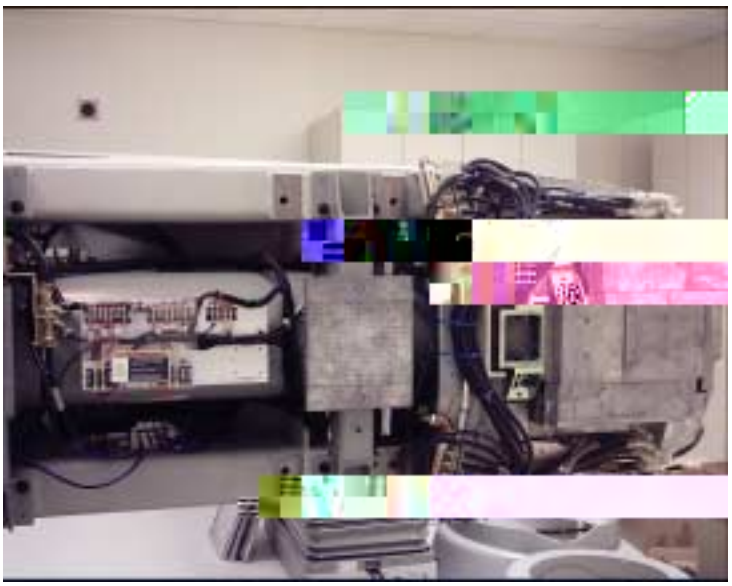

Accelerator Tube (different view)

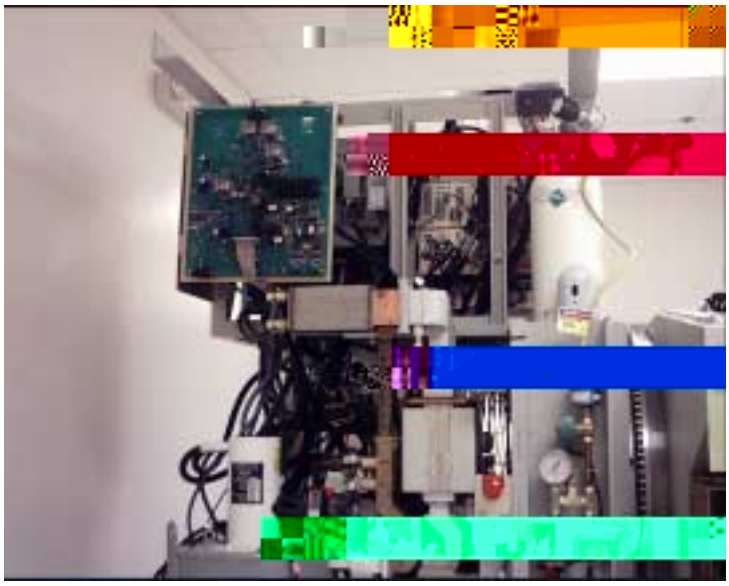

Ancillary Equipment

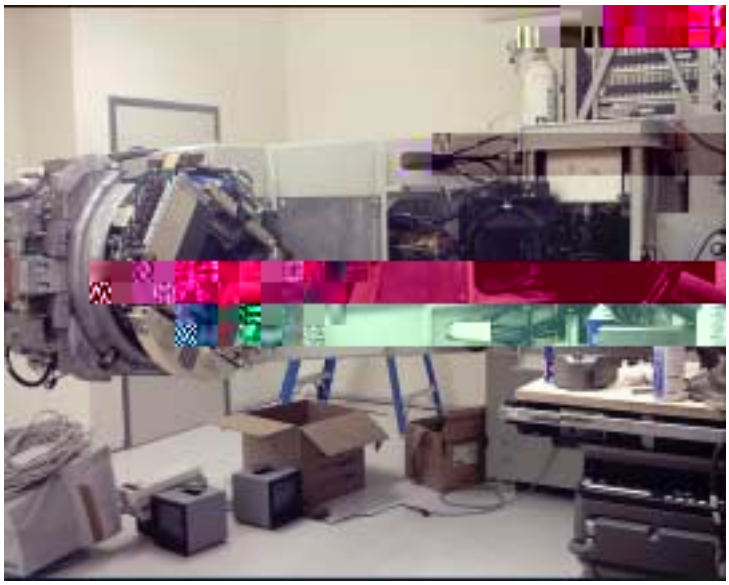

Gantry

Appendix B. DICOM to TIFF Application

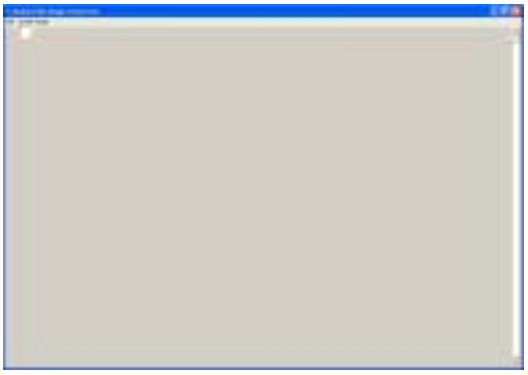

Opened Application

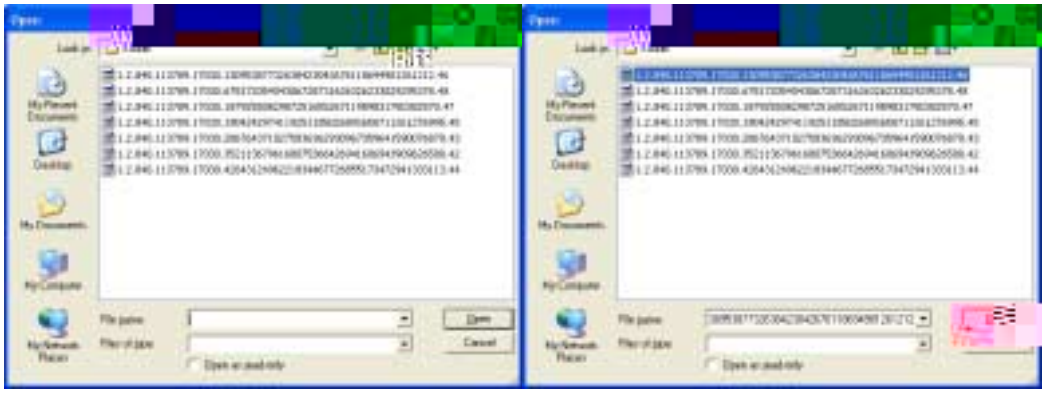

Opening Kodak Image File

Opened Kodak Image File

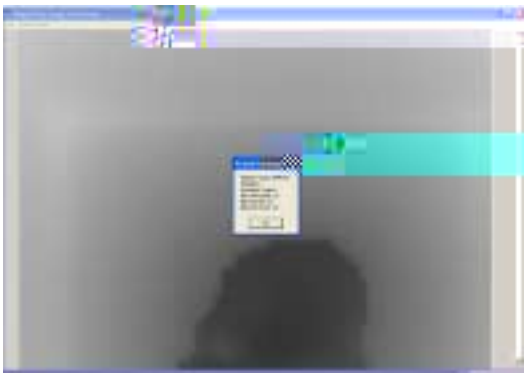

Getting the Header Information of the Image

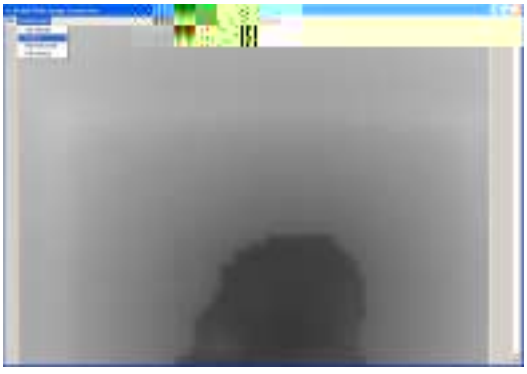

Inverting the Image

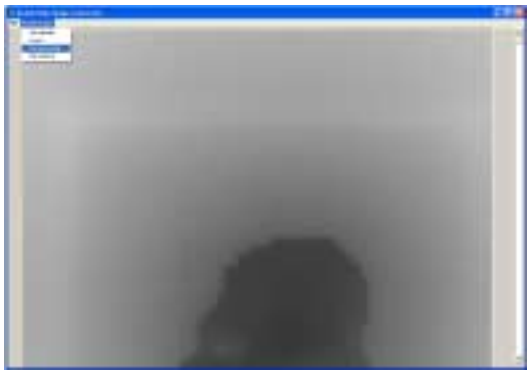

Flipping the Image Horizontally

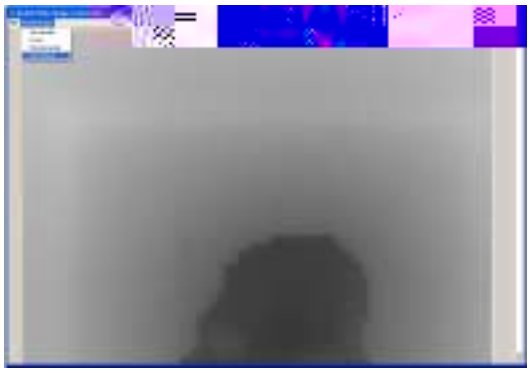

Flipping the Image Vertically

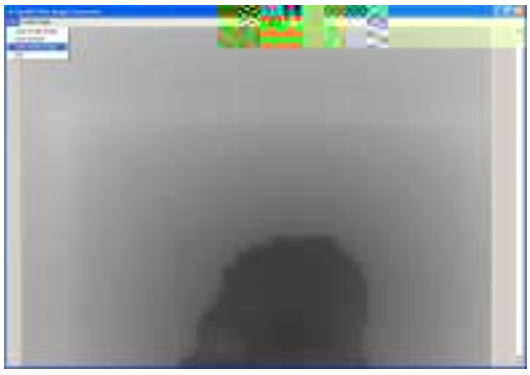

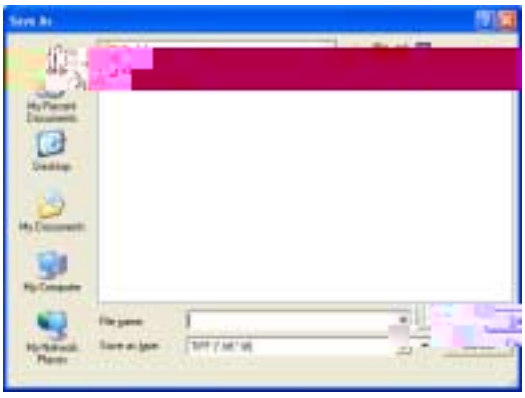

Saving the Image in TIFF Format

Appendix C. MU Calculations

Monitor Unit Calculation for Photon Beam

Dosimetric quantities used in the calculation are[24]:

- TMR (Tissue-Maximum Ratio)
    - special case of TPR (tissue-phantom ratio)
    - ratio of dose at a given point in phantom (point P) to the dose at the same point in the beam (point Q) at a fixed reference depth of maximum dose, d_m, Figure 45

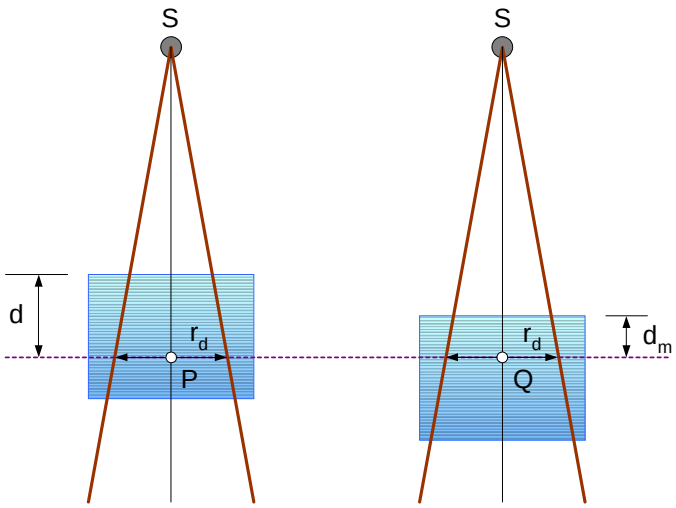

Figure 45. Definition of TMR

- TMR can be derived directly from the percent depth dose (PDD) data

where r is field size at surface, r_d is field size at depth d, SSD is source-surface distance and $_p$

Appendix D. Interpolation in Image Processing

Interpolation in Image Processing

Interpolation is the process used to estimate an image value at a location in between image pixels. For example, if image is resized so it contains more pixels than it did originally, interpolation is used to determine the values for the additional pixels.

Three interpolation methods most commonly used in image processing are:

- Nearest-neighbor interpolation
- Bilinear interpolation
- Bicubic interpolation

They all work in fundamentally similar way.

Nearest neighbor interpolation offers fast method of resampling but it only takes info from pixels at each side of the new one so the calculation is less precise. The output pixel is assigned value the point falls within, no other pixels are considered.

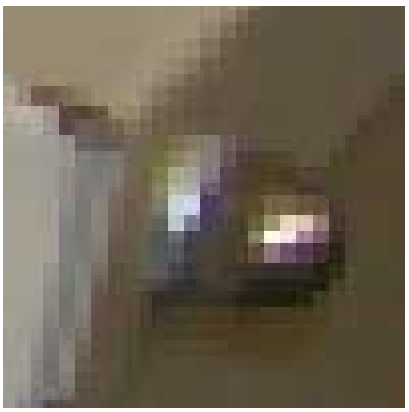

Bilinear interpolation takes info from the pixels above and to the side of where the new pixel will appear and offers slightly better quality when compared to nearest neighbor interpolation. The output pixel is a weighted average of pixels in the nearest 2 by 2 neighborhood.

Appendix E. Fourier Transform

Fourier Transform

In 1807, Jean Baptiste Joseph Fourier presented the results of his study of heat propagation and diffusion to the ‘Institut de France’. In his presentation, he claimed that any

118The Fourier transform of a 2-dimensional function is shown mathematically as Eq.0113

phase of the sine and cosine waves. This information along with the frequency, allows full

transform is performed. There are a number of window functions, each with its set of advantages and disadvantages. Window functions attenuate the original image data.

The discrete Fourier transform is computationally intensive. An image of size $M \times M$ will require $(M^2)^2$ or M^4 complex multiplications. Fortunately, in 1942, it was discovered that the discrete Fourier transform of length N could be rewritten as the sum of two Fourier transforms of length $N/2$. This technique is known as the Fast Fourier Transform. It reduces the number of complex multiplications from N^2 to the order of $N\log_2 N$. This savings is substantial especially when image processing is done. The FFT is separable, which makes Fourier transforms even easier to do. Because of the separability, the FFT operation can be reduced from a 2-dimensional operation to two 1-dimensional operations. First the FFT of the rows of an image is computed and then the FFT of the columns. For an image of size $M \times N$, this requires $N + M$ FFTs to be computed. The order of

Appendix F. Determination of the Translation, Rotation and Scaling Values

Determination of the translation value

(*Note:* in accordance with the terminology used previously, $I(\dot{x}) = I(x, y)$ and $F(\omega) = H(u, v)$)

It is known that if two images, $I1(\dot{x})$ and

In the ideal case the absolute value of the ratio is equal to 1. In real life images have some noise in them. In the presence of noise observed values of the intensities may differ from the actual values, and as a result the absolute value of the ratio $R(\omega'')$ may be different from 1. To find out exact value of the ratio in the presence of noise following can be done. Let

$e^{-2\pi i(\omega'' a)} = b$

then in absence of noise:

Eq. 20 $F2(\omega'') = bF1(\omega'')$

In the presence of noise Fourier transforms, $F1(\omega)$ and $F2(\omega)$, can be different from the actual values so the Eq. 20 changes to

Eq. 21 $F2(\omega'') \approx bF1(\omega'')$

As stated before it is also known that absolute value of b is equal to 1:

Eq. 22

Then among all estimates that satisfy the additional condition in Eq. 22, a value of b for which the square of error, $|E|^2 = E \cdot E^*$, is minimum is found. Knowing

Eq. 24

$$|E|^2 = E \cdot E^* = \left[F2(\omega'') - bF1(\omega'')\right] \cdot \left[F2^*(\omega'') - b^* F1^*(\omega'')\right]$$
$$= F2(\omega'')F2^*(\omega'') - b^* F2(\omega'')F1^*(\omega'') - bF1(\omega'')F2^*(\omega'') + bF1(\omega'')b^* F1^*(\omega'')$$

Resulting expression has to be minimized under the constraint in Eq. 22.[9] Constraint optimization is the minimization of an objective function subject to constraints on the possible values of the independent variable. The typical constrained optimization problem has the following form:

$\min_x \{f(x)\}$ subject to $g(x) = 0$

where $f(x)$ is the scalar-valued objective function and $g(x)$ is the vector-valued constraint function.

The classical approach to solving constraint optimization problems is the method of Lagrange Multipliers. This approach converts the constrained optimization problem into an unconstrained one. The Lagrangian of a constraint optimization problem is defined to be the scalar-valued function

$L(x, \lambda) = f(x) + \lambda^T g(x)$

where λ is Lagrange multiplier.

Stationary points of the Lagrangian are potential solutions of the constrained optimization problem, as always each candidate solution must be tested to determine which one minimizes the objective function. As shown in Figure 48, the constraint corresponds to a contour in the x plane.

From this equation b can be found as

Eq. 27 $$b = \frac{F2_{II}^{\cdot\cdot}(\omega)F1_{II}^{*\cdot\cdot}(\omega)}{F1(\omega)F1^{*}(\omega)+\lambda}$$

From the condition in Eq. 22 that value b should satisfy the coefficient

the other values of this function. In this case desired shift a represents the point for which the absolute value of the inverse Fourier transform takes the largest possible value.

Using Log-Polar Coordinates for the Determination of Rotation and Scaling Values

If one image differs from another not only by shift, but also by the rotation and scaling then the absolute values (magnitudes) of their Fourier transforms are not equal, but also differ by the corresponding rotation and scale.

If $I(x, y)$ is an image with support on a rectangular set in the Euclidean plane, then the log-polar transform with origin (x_0, y_0) is described by following mapping[19]:

$\xi = M \log(r + \alpha)$ **SC2 Jw(j0.495 w 10 M 0 d96 13.5)Tj1424F2 1 m180T4 1 4.99 lS6.9671j35**

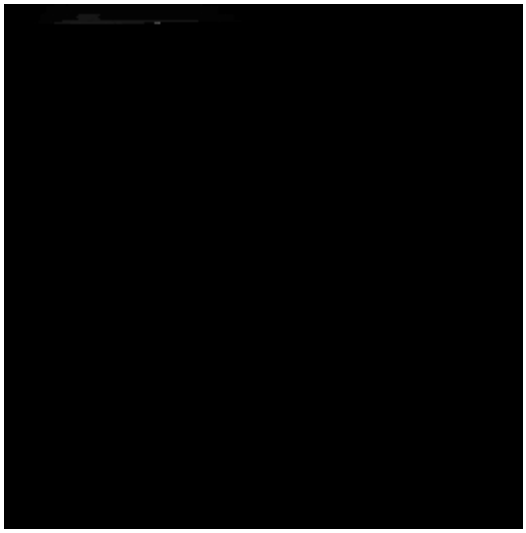

Original Image

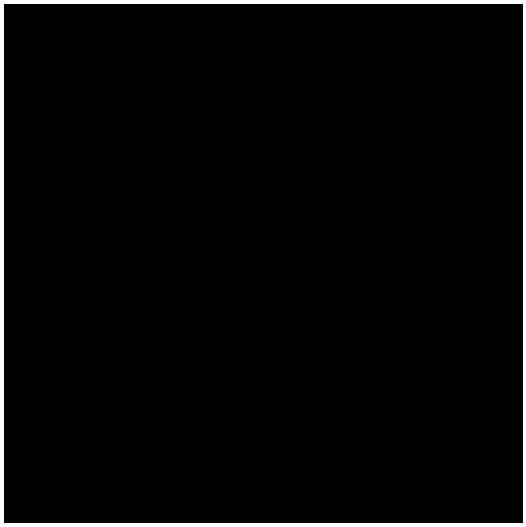

The Original Image Overlayed with Log-Polar Grid

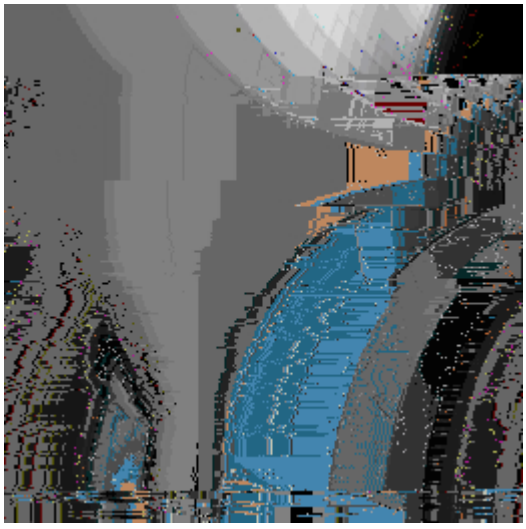

Generated Log-Polar Image

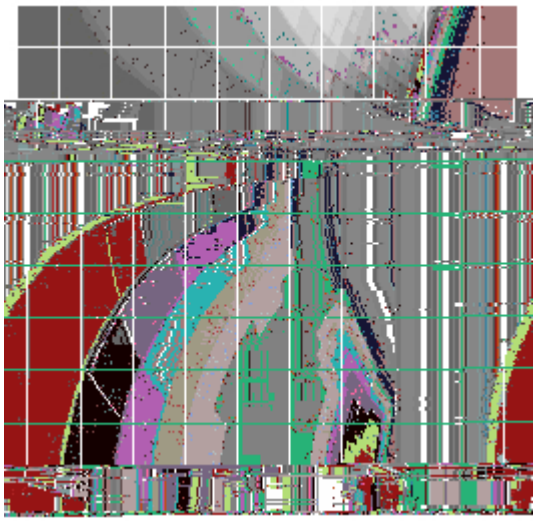

Log-Polar Image with the Rectilinear Grid Overlay

Figure 50. Log-polar imaging

After log-polar image is mapped back to Cartesian coordinates the decrease in resolution with increasing radius can be observed.

Determining Rotation and Scaling

Log-polar transformation can be used to describe both rotation and scaling as a shift. To determine rotation and scaling needed for the image registration both images have to be transformed from the original Cartesian coordinates to log-polar coordinates. Next same Fourier transforms as described for the translation determination are used to determine the corresponding shift $(\theta_0, \log(\lambda))$, from these values rotation angle θ_0 and scaling factor λ are reconstructed.

However, computing (ξ, η) from the original rectangular grid leads to points that are not located exactly at points in the original grid. Thus, interpolation is needed to find a value of $abs(F(\omega))$ on the desired grid. A bilinear interpolation is used for resampling. Knowing the transformation relationship between the log-polar plane and Cartesian plane, point (x, y) in Cartesian plane is related to the desired grid point (ξ, η) by

Eq. 32

$$x = r\cos(\eta) = 10^{\xi}\cos(\eta)$$
$$y = r\sin(\eta) = 10^{\xi}\sin(\eta)$$

Relations used:

Eq. 34

$$x_0 = floor(x) \qquad x_1 = x_0 + 1$$
$$y_0 = floor(y) \qquad y_1 = y_0 + 1$$

$$A(x, y_0) = (x_1 - x)A(x_0, y_0) + (x - x_0)A(x_1, y_0)$$

and

$$A(x, y_1) = (x_1 - x)A(x_0, y_1) + (x - x_0)A(x_1, y_1)$$

so finally

Eq. 35

$$(\quad , \quad) \quad (\quad _1 \quad) \quad (\quad , \quad _0) \quad (\quad \quad _0) \quad (\quad , \quad _1)$$

$$(\quad , \quad) \quad (\quad _1 \quad)(\quad _1 \quad \quad) \quad (\quad _0 , \quad _0) \quad (\quad _1 \quad)(x \quad x_0)A(x_1, y_0)$$
$$(y \quad y_0)(x_1 \quad x)A(x_0, y_1) \quad (y \quad y_0)(x \quad x_0)A(x_1, y_1)$$

Appendix G. Film Calibration Behavior

Several calibration files, generated from calibration films exposed and scanned on different days by the RIT113 system, were analyzed.

Presented here are results obtained for different energies. Differences depending on the date of the scan are clearly visible, meaning that one calibration curve for particular energy would not probably do and showing very clearly why every time exposure of film is done calibration curve needs to be generated too. Results for only 2 energies are presented (4 and 10 MV), but analysis was done for 6 and 15 MV too showing the same amount of discrepancy. All the values compared come from the same machine.

4 MV	10 MV

4 MV				10 MV			
Dose (cGy)	**Date of Scan**	**Value Read by RIT113**	**% difference (min-max)**	**Dose (cGy)**	**Date of Scan**	**Value Read by RIT113**	**% difference (min-max)**
50	6/16/2003 10/23/2003 7/2/2003 9/19/2003 12/3/2003 9/8/2003 5/29/2003 2/10/2004	379 149 391 469 376 975 366 498	84	56	7/28/2003 4/1/2003 8/8/2003 6/23/2003 7/17/2003 03/18/2003 2/11/2003 5/29/2003 2/3/2003 4/21/2003 1/5/2004 4/19/2004 4/14/2004	273 224 190 212 230 213 189 204 190 198 194 254 361	48
34	6/16/2003 10/23/2003 7/2/2003 9/19/2003 12/3/2003 9/8/2003 5/29/2003 2/10/2004	1037 423 1001 1128 1041 1698 977 1322	75	37	7/28/2003 4/1/2003 8/8/2003 6/23/2003 7/17/2003 03/18/2003 2/11/2003 5/29/2003 2/3/2003 4/21/2003 1/5/2004 4/19/2004 4/14/2004	774 673 559 624 631 695 522 633 586 619 649 741 981	43
17	6/16/2003 10/23/2003 7/2/2003 9/19/2003 12/3/2003 9/8/2003 5/29/2003 2/10/2004	2106 1612 2101 2098 2075 2309 2099 2179	30	19	7/28/2003 4/1/2003 8/8/2003 6/23/2003 7/17/2003 03/18/2003 2/11/2003 5/29/2003 2/3/2003 4/21/2003 1/5/2004 4/19/2004 4/14/2004	1954 1950 1808 1857 1880 1946 1787 1857 1833 1905 1825 1979 2117	16
0	6/16/2003 10/23/2003 7/2/2003 9/19/2003 12/3/2003 9/8/2003 5/29/2003 2/10/2004	3434 3138 3367 3369 3333 3250 3413 3280	9	0	7/28/2003 4/1/2003 8/8/2003 6/23/2003 7/17/2003 03/18/2003 2/11/2003 5/29/2003 2/3/2003 4/21/2003 1/5/2004 4/19/2004 4/14/2004	3323 3483 3442 3360 3213 3444 3440 3394 3484 3470 3420 3522 3544	9

Appendix H. CR Plate Calibration Values

Calibration curve values are presented hereafter together with the exponential equations generated as a trendline fit through the data points measured for different maximum values of monitor units delivered.

Different color means that exposure was done on different day.

4 MV

MU	Dose (cGy)	RGB	MU	Dose (cGy)	RGB	MU	Dose (cGy)	RGB	MU	Dose (cGy)	RGB
1	0.84	162	31	25.98	72	67	56.15	54	105	87.99	43
2	1.68	145	32	26.82	71	68	56.99	52	106	88.83	44
2	1.68	149	33	27.66	71	69	57.83	54	107	89.67	42
3	2.51	136	34	28.49	71	70	58.66	53	108	90.51	43
4	3.35	129	35	29.33	69	70	58.66	51	109	91.35	45
5	4.19	122	35	29.33	71	71	59.50	51	110	92.19	43
5	4.19	116	36	30.17	69	72	60.34	51	110	92.19	44
5	4.19	123	37	31.01	68	73	61.18	53	111	93.02	44
6	5.03	119	38	31.85	66	74	62.02	50	112	93.86	43

6 MV

MU	Dose (cGy)	RGB	MU	Dose (cGy)	RGB	MU	Dose (cGy)	RGB	MU	Dose (cGy)	RGB
1	0.87	167	28	24.30	79	62	53.82	58	100	86.80	53
1	0.87	163	29	25.17	78	63	54.68	57	101	87.67	48

1.7(f04

4 MV

monitor units	SpSc(5x5)	TMR(5,5)	Dose (cGy)
20	0.946	0.865	16.8
40	0.946	0.865	33.5
60	0.946	0.865	50.3
80	0.946	0.865	67.0
100	0.946	0.865	83.8
120	0.946	0.865	100.6

Equations used depending on the maximum dose delivered (that is obtained from the plan image) and MUs read from the table above:

up to 20

RGB

10 MV

monitor units	SpSc(5x5)	TMR(5,5)	Dose (cGy)
20	0.935	0.950	18.7
40	0.935	0.950	37.3
50	0.946	0.865	41.9

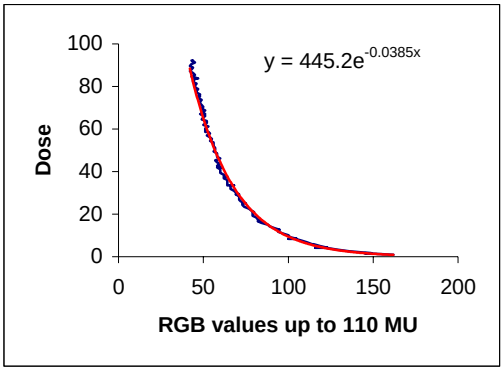

Up to 110 MU

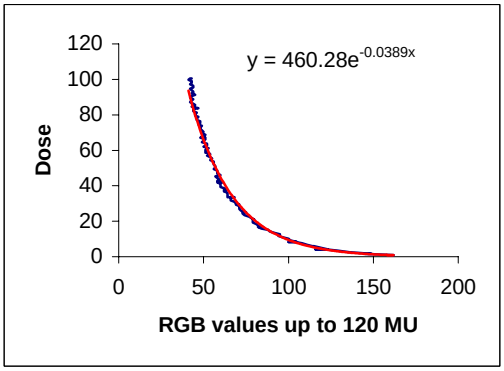

Up to 120 MU

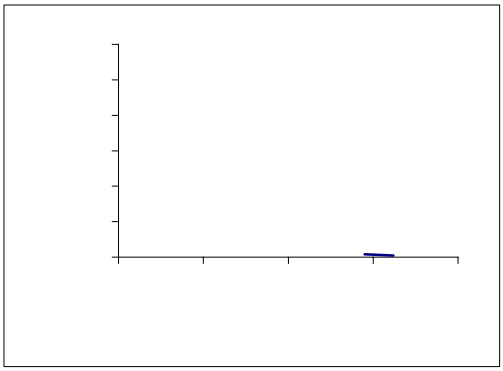

6 MV curves

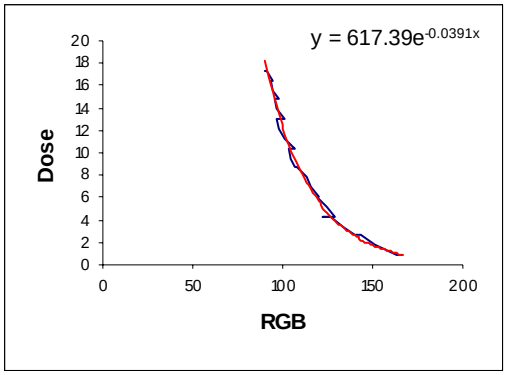
y = 617.39e-0.0391x
Dose
RGB
0
2
4
6
8
10
12
14
16
18
20
0
50
100
150
200

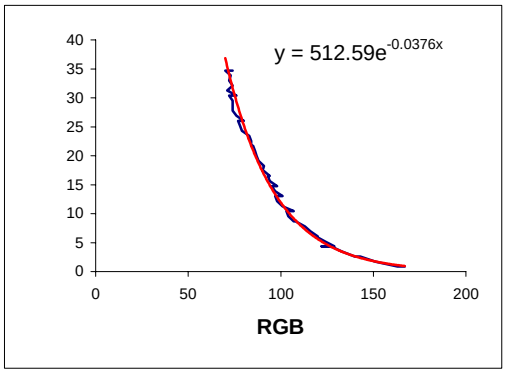
y = 512.59e-0.0376x
RGB
0
5
10
15
20
25
30
35
40
0
50
100
150
200

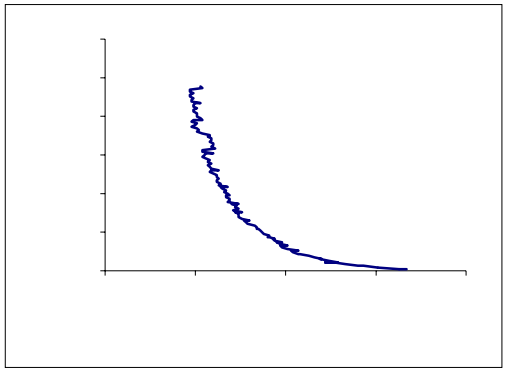

Graph below shows comparison of the calibration curves for three different energies using the

Vita

Ines-Ana Jurkovic is from Croatia, Europe. She studied at Faculty of Electrical

Other work experience in February-July 1998 includes work in the Department of the Environmental Quality, Louisiana Radiation Protection Division, USA, on emergency planning, response and preparedness issues.

Awards received include Award for Excellent Work in technical field from the Ecole Polyvalente Technique "Armand Corbeil", Canada, 1985; "Josip Lon